Universität Stuttgart

The equivalence of standard and mixed finite element methods in applications to elasto-acoustic interaction

B. Flemisch, M. Kaltenbacher, S. Triebenbacher, B. Wohlmuth

Berichte aus dem Institut für Angewandte Analysis und Numerische Simulation

Preprint 2009/004

Universität Stuttgart

The equivalence of standard and mixed finite element methods in applications to elasto-acoustic interaction

B. Flemisch, M. Kaltenbacher, S. Triebenbacher, B. Wohlmuth

Berichte aus dem Institut für Angewandte Analysis und Numerische Simulation

Preprint 2009/004

Institut für Angewandte Analysis und Numerische Simulation (IANS)
Fakultät Mathematik und Physik
Fachbereich Mathematik
Pfaffenwaldring 57
D-70 569 Stuttgart

E-Mail: ians-preprints@mathematik.uni-stuttgart.de
WWW: http://preprints.ians.uni-stuttgart.de

ISSN **1611-4176**

THE EQUIVALENCE OF STANDARD AND MIXED FINITE ELEMENT METHODS IN APPLICATIONS TO ELASTO-ACOUSTIC INTERACTION

BERND FLEMISCH*, MANFRED KALTENBACHER†, SIMON TRIEBENBACHER†, AND BARBARA I. WOHLMUTH‡

Abstract. Two commonly used problem formulations for the description of acoustic wave propagation are investigated, one based on the fluid displacement and the other one based on the velocity potential as primary variable. Their equivalence under general Neumann boundary conditions is shown both on the continuous and discrete level. To obtain the equivalence in the discrete setting, a non-standard mixed finite element formulation is introduced. Thus, the transfer of an already available analysis for coupled elasto-acoustic problems in the displacement formulation to the potential formulation can be achieved. For the applications, the potential formulation is of special interest, because it allows the use of standard Lagrangian elements in both the stucture and the fluid subdomain. Moreover, the approach does not require any conformity of the subdomain meshes at the interface, which considerably simplifies the physics-adapted mesh generation. Several engineering examples demonstrate the applicability and efficiency of the resulting numerical scheme.

1. Introduction and preliminary results. Many engineering problems deal with the interaction of vibrating mechanical structures and acoustic fields. E.g., piezoelectric and capacitive micro-machined ultrasound transducers for medical imaging and nondestructive testing, sound transducers as electrodynamic and piezoelectric loudspeakers as well as capacitive microphones, noise shielding and cancellation systems to mention just some [17, 14]. Since we deal with a coupled field problem - in our case the interaction between the mechanical and acoustic field - we have to be very careful when setting up the formulation on the continuous and furthermore then on the discrete level. Various aspects of domain decomposition techniques come into play like interface conditions between different types of variables and non-matching meshes.

While it is standard to use a displacement based formulation for the elastic part, a variety of formulations depending on the choice of the primary variable exists for the acoustic part. In particular, one can choose a formulation based on pressure, [21], displacement potential, [18], velocity potential, [14], or on the vector-valued fluid displacements, [3]. This may result in different Hilbert spaces for the weak formulations, namely, H^1 and H^{div}, and thus different finite element spaces for the discretizations. We base our formulation on the primary variables mechanical displacement and acoustic velocity potential, since this choice allows us to use on both subdomains standard Lagrange finite elements. Moreover, the coupled formulation remains symmetric [20]. In order to gain full flexibility for the discretization, we use possibly non-matching grids along the coupling interface. Therewith, the mesh generation process gets much easier, since grids in different sub-domains do not influence each other, and we obtain the possibility to choose the grid size optimal for both physical fields.

However, the analysis of the coupled time-dependent problem is not straightforward, since standard results on evolution equations cannot be applied, [9, 10, 16, 23]. In contrast, the stability analysis for the purely displacement based formulation employing Raviart–Thomas finite elements is already available, [3]. By showing the equivalence between these two formulations both in the continuous and in the discrete setting, we obtain existence and uniqueness of our formulation. This provides a sound theoretical foundation for the engineering approach used in [14].

To demonstrate the efficiency and applicability of our implementation, we present several applications such as an electrodynamic loudspeaker as well as ultrasound wave generation by multiple plates as used in capacitive micro-machined ultrasound transducers. The use of non-matching grids along the coupling interface strongly improves the quality of the meshes in both sub-domains and the overall computational efficiency. We note that our concept can be easily

*Institut für Wasserbau (IWS), Universität Stuttgart, Pfaffenwaldring 61, 70569 Stuttgart, Germany. email: flemisch@iws.uni-stuttgart.de

†Institute of Smart Systems Technologies, Alpen-Adria University of Klagenfurt, Austria. email: {Manfred.Kaltenbacher,Simon.Triebenbacher}@uni-klu.ac.at

‡Institute of Applied Analysis and Numerical Simulations (IANS), Universität Stuttgart, Pfaffenwaldring 57, 70529 Stuttgart, Germany. email: wohlmuth@ians.uni-stuttgart.de

This work was supported by the Deutsche Forschungsgemeinschaft, KA 1638/2-1, WO 671/6-1.

generalized to more complex subdomain models and to higher order finite elements, which we will show in our last example of a piezoelectric loudspeaker.

The rest of the paper is organized as follows. In the rest of this introduction, we state an elementary result for H^{div} functions based on the Helmholtz decomposition. Section 2 introduces a potential based and an equivalent displacement based continuous formulation for the acoustic subproblem. The main theoretical result is given in Section 3, where we introduce two equivalent discrete schemes. While the discretization for the potential formulation is based on standard Lagrange finite elements, the one for the displacement formulation employs non-standard mixed finite elements. Moreover, an optimal a priori error estimate for the mixed method is shown. In Section 4, the coupled elasto-acoustic problem formulations are given with special focus on the interface conditions. Finally, Section 5 provides applications of the discrete coupled problems to several engineering applications.

Let $\Omega \subset \mathbb{R}^d$, $d = 2, 3$, denote a bounded domain with outward unit normal $\boldsymbol{\nu}$. By $(\cdot,\cdot)_\Omega$, we indicate the L^2-inner product of scalar or vector-valued functions on Ω, and set $\|\cdot\|_{0,\Omega}^2 = (\cdot,\cdot)_\Omega$. Moreover, we introduce the spaces V_d by setting with $V_2 = H_0^1(\Omega)$ the standard space of scalar L^2-functions with L^2-gradients, and with $V_3 = (H_0^1(\Omega))^3$ the corresponding space of vector fields. From now on, our notation of function spaces will not be different for spaces of scalar functions or vector fields. However, in general, we will distinguish elements of these spaces by using greek letters in normal font and latin letters in bold font, respectively. Nevertheless, we will use late-alphabet greek letters for elements in V_d which can be scalar or vector-valued, depending on the dimension d. Additionally, we set

$$H^{\mathrm{div}}(\Omega) = \{\boldsymbol{v} \in L^2(\Omega) : \operatorname{div} \boldsymbol{v} \in L^2(\Omega)\},$$
$$H_0^{\mathrm{div}}(\Omega) = \{\boldsymbol{v} \in H^{\mathrm{div}}(\Omega) : \boldsymbol{v}\cdot\boldsymbol{\nu} = 0 \text{ on } \partial\Omega\},$$

and the associated norm $\|\cdot\|_{\mathrm{div},\Omega}^2 = (\cdot,\cdot)_\Omega + (\operatorname{div}\cdot, \operatorname{div}\cdot)_\Omega$. We will frequently make use of the following standard result.

LEMMA 1.1. *Assume that $\Omega \subset \mathbb{R}^d$ is simply connected for $d = 3$ or that the boundary $\partial\Omega$ is connected for $d = 2$. Let $\boldsymbol{w} \in L^2(\Omega)$ satisfy*

$$(\boldsymbol{w}, \mathbf{curl}\,\tau)_\Omega = 0, \qquad \tau \in V_d. \tag{1.1}$$

i) Then $\boldsymbol{w} = \operatorname{grad}\alpha$ for a function $\alpha \in \widetilde{H}^1(\Omega) = \{\phi \in H^1(\Omega) : (\phi, 1)_\Omega = 0\}$.
ii) If additionally $\boldsymbol{w} \in H_0^{\mathrm{div}}(\Omega)$, it holds that

$$\|\boldsymbol{w}\|_{\mathrm{div},\Omega} \sim \|\operatorname{div}\boldsymbol{w}\|_{0,\Omega}.$$

Proof. For convenience of the reader, we recall the proof. The Helmholtz decomposition admits to write $\boldsymbol{w} \in L^2(\Omega)$ as $\operatorname{grad}\alpha + \mathbf{curl}\,\tau$ with $\alpha \in \widetilde{H}^1(\Omega)$, $\tau \in V_d$, [27, (A.6), (A.18), (A.21)]. We note that $\operatorname{grad} H^1 \perp \mathbf{curl}\, V_d$, and thus

$$\|\boldsymbol{w}\|_{0,\Omega}^2 = \|\operatorname{grad}\alpha\|_{0,\Omega}^2 + \|\mathbf{curl}\,\tau\|_{0,\Omega}^2.$$

Due to (1.1), we find

$$\|\mathbf{curl}\,\tau\|_{0,\Omega}^2 = (\boldsymbol{w} - \operatorname{grad}\alpha, \mathbf{curl}\,\tau)_\Omega = 0,$$

which yields i). Moreover, if $\boldsymbol{w}$ is also in $H_0^{\mathrm{div}}(\Omega)$, we find that

$$\|\operatorname{grad}\alpha\|_{0,\Omega}^2 = -(\operatorname{div}\boldsymbol{w}, \alpha)_\Omega \le \|\operatorname{div}\boldsymbol{w}\|_{0,\Omega}\|\alpha\|_{0,\Omega} \le C\|\operatorname{div}\boldsymbol{w}\|_{0,\Omega}\|\operatorname{grad}\alpha\|_{0,\Omega}.$$

In the last step, we have used that the H^1-seminorm restricted to $\widetilde{H}^1(\Omega)$ is equivalent to the H^1-norm. $\square$

2. Continuous acoustic problem formulations. This section investigates the continuous acoustic problems. We first introduce the two problem formulations in Subsections 2.1 and 2.2. Then, we state the compatibility conditions which admit the equivalence of the problems in Subsection 2.3. The equivalence is actually shown in the final Subsection 2.4.

2.1. Potential-based formulation. Our goal is to model the propagation of acoustic waves inside a bounded domain Ω^{a} with boundary $\Gamma = \partial\Omega^{\mathrm{a}}$. One possibility is to use the linear wave equation for the acoustic velocity potential ψ. Given $T > 0$ and the speed of sound $c \in L^\infty(\Omega^{\mathrm{a}})$, one seeks ψ such that

$$c^{-2}\ddot{\psi} - \operatorname{div}\operatorname{grad}\psi = 0 \quad \text{in } \Omega^{\mathrm{a}} \times (0,T),$$

which is complemented by the natural boundary condition

$$\operatorname{grad}\psi \cdot \boldsymbol{\nu} = -v_{\boldsymbol{\nu}} \quad \text{on } \Gamma \times (0,T), \tag{2.1}$$

and initial conditions

$$\psi(0) = \psi^0 \quad \text{and} \quad \dot{\psi}(0) = \psi^1 \quad \text{in } \Omega^{\mathrm{a}}. \tag{2.2}$$

The reason for choosing the boundary condition (2.1) is that for the coupled elasto-acoustic problem investigated in Section 4, relation (2.1) enforces the continuity of the normal velocity.

Transforming to the variational setting, we employ the common Sobolev space framework and notation for evolution problems, [9, 10, 16, 23]. Abbreviating the notion $W(0,T;V)$ by $W(V)$ for indicating the regularity with respect to time and space, and denoting by $\langle\cdot,\cdot\rangle_{1,\Omega^{\mathrm{a}}}$ and $\langle\cdot,\cdot\rangle_{1/2,\Gamma}$ the duality product on $H^{-1}(\Omega^{\mathrm{a}}) \times H^1(\Omega^{\mathrm{a}})$ and $H^{-1/2}(\Gamma) \times H^{1/2}(\Gamma)$, respectively, we arrive at:

Problem 2.1. *Given $\psi^0 \in H^1(\Omega^{\mathrm{a}})$, $\psi^1 \in L^2(\Omega^{\mathrm{a}})$, $v_{\boldsymbol{\nu}} \in L^2(H^{-1/2}(\Gamma))$, find an acoustic velocity potential $\psi \in L^2(H^1(\Omega^{\mathrm{a}}))$ such that*

$$\langle c^{-2}\ddot{\psi}(\cdot), \phi\rangle_{1,\Omega^{\mathrm{a}}} + (\operatorname{grad}\psi(\cdot), \operatorname{grad}\phi)_{\Omega^{\mathrm{a}}} = -\langle v_{\boldsymbol{\nu}}(\cdot), \phi\rangle_{1/2,\Gamma}, \quad \phi \in H^1(\Omega^{\mathrm{a}}), \tag{2.3}$$

in the sense of distributions on $(0,T)$, together with the initial conditions (2.2).

2.2. Displacement-based formulation. Instead of taking the velocity potential as primary variable for the acoustic domain Ω^{a}, one can seek the displacement field $\boldsymbol{u}_{\mathrm{a}}$ such that

$$\ddot{\boldsymbol{u}}_{\mathrm{a}} - \operatorname{grad}(c^2 \operatorname{div}\boldsymbol{u}_{\mathrm{a}}) = 0 \quad \text{in } \Omega^{\mathrm{a}} \times (0,T),$$

complemented by the essential boundary condition

$$\boldsymbol{u}_{\mathrm{a}} \cdot \boldsymbol{\nu} = u_{\boldsymbol{\nu}} \quad \text{on } \Gamma \times (0,T), \tag{2.4}$$

and the initial conditions

$$\boldsymbol{u}_{\mathrm{a}}(0) = \boldsymbol{u}_{\mathrm{a}}^0 \quad \text{and} \quad \dot{\boldsymbol{u}}_{\mathrm{a}}(0) = \boldsymbol{u}_{\mathrm{a}}^1 \quad \text{in } \Omega^{\mathrm{a}}. \tag{2.5}$$

We assume that the mean density of the acoustic fluid is constant. For the upcoming elasto-acoustic problem, the essential boundary condition (2.4) corresponds to the continuity of the normal displacements.

Using the boundary condition (2.4), we define

$$L^2(H^{\mathrm{div}}_*(\Omega^{\mathrm{a}})) = \{\boldsymbol{v} \in L^2(H^{\mathrm{div}}(\Omega^{\mathrm{a}})) : \boldsymbol{v}\cdot\boldsymbol{\nu} = u_{\boldsymbol{\nu}} \text{ on } \Gamma \times (0,T)\}. \tag{2.6}$$

The resulting weak problem reads as follows.

Problem 2.2. *Given $\boldsymbol{u}_{\mathrm{a}}^0 \in H^{\mathrm{div}}(\Omega^{\mathrm{a}})$, $\boldsymbol{u}_{\mathrm{a}}^1 \in L^2(\Omega^{\mathrm{a}})$, $u_{\boldsymbol{\nu}} \in L^2(H^{-1/2}(\Gamma))$, find an acoustic displacement field $\boldsymbol{u}_{\mathrm{a}} \in L^2(H^{\mathrm{div}}_*(\Omega^{\mathrm{a}}))$ such that*

$$\langle \ddot{\boldsymbol{u}}_{\mathrm{a}}(\cdot), \boldsymbol{v}\rangle_{\mathrm{div},\Omega^{\mathrm{a}}} + (c^2\operatorname{div}\boldsymbol{u}_{\mathrm{a}}(\cdot), \operatorname{div}\boldsymbol{v})_{\Omega^{\mathrm{a}}} = 0, \qquad \boldsymbol{v} \in H^{\mathrm{div}}_0(\Omega^{\mathrm{a}}), \tag{2.7}$$

in the sense of distributions on $(0,T)$, together with the initial conditions (2.5).

Remark 2.3. *In our coupled formulation, the boundary data $u_{\boldsymbol{\nu}}$ will be of higher spatial regularity $H^{1/2}(\Gamma)$ due to the fact that $u_{\boldsymbol{\nu}}$ is assumed to coincide with the restriction of H^1-regular diplacements from the solid domain onto the interface Γ.*

2.3. Continuous compatibility conditions. The equivalence of Problems 2.1 and 2.2 can only be guaranteed if both the boundary and the initial data are compatible. In this section, we will discuss the compatibility conditions in detail. While the condition for the boundary data is inherited from the underlying coupled elasto-acoustic problem, we explicitly construct initial data for the displacement Problem 2.2 which is compatible to a given initial solution for the potential Problem 2.1. From now on, the subscript "a" is frequently omitted from $\boldsymbol{u}_{\mathrm{a}}$ whenever it is unambiguous.

2.3.1. Boundary data. For the elasto-acoustic problem, the solid displacements result in compatible boundary data $v_{\boldsymbol{\nu}}$ and $u_{\boldsymbol{\nu}}$, in particular,

- natural conditions for Problem 2.1 for the velocity potential, incorporated in the variational equality (2.3), and
- essential conditions for Problem 2.2 for the acoustic displacements, incorporated in the definition of the space $L^2(H_*^{\mathrm{div}}(\Omega^{\mathrm{a}}))$ in (2.6).

Since for the moment no coupling to the solid domain is assumed, we just impose the required compatibility by assuming that

$$\langle v_{\boldsymbol{\nu}}(\cdot), \phi\rangle_{1/2,\,\Gamma} = \langle \dot{u}_{\boldsymbol{\nu}}(\cdot), \phi\rangle_{1/2,\,\Gamma}, \quad \phi \in H^{1/2}(\Gamma) \tag{2.8}$$

in the sense of distributions on $(0, T)$.

2.3.2. Initial data. The compatibility of the initial data is provided by means of the following lemma.

Lemma 2.4. *Let the initial and boundary data ψ^0, ψ^1, and $v_{\boldsymbol{\nu}}$ of Problem 2.1 be given. Let also the boundary data $u_{\boldsymbol{\nu}}$ of Problem 2.2 satisfying* (2.8) *be given and assume additionally that*

$$-(c^{-2}\psi^1, 1)_{\Omega^{\mathrm{a}}} = \langle u_{\boldsymbol{\nu}}(0), 1\rangle_{\Gamma}. \tag{2.9}$$

Then, initial data $\boldsymbol{u}^0 \in H^{\mathrm{div}}(\Omega^{\mathrm{a}})$, $\boldsymbol{u}^1 \in L^2(\Omega^{\mathrm{a}})$ of Problem 2.2 can be uniquely selected by requiring

$$\operatorname{div} \boldsymbol{u}^0 = -c^{-2}\psi^1 \text{ in } \Omega^{\mathrm{a}}, \qquad \boldsymbol{u}^0 \cdot \boldsymbol{\nu} = u_{\boldsymbol{\nu}}(0) \text{ on } \Gamma, \tag{2.10}$$

$$(\boldsymbol{u}^0, \mathbf{curl}\, \tau)_{\Omega^{\mathrm{a}}} = 0, \quad \tau \in V_d, \tag{2.11}$$

$$\boldsymbol{u}^1 = -\operatorname{grad} \psi^0 \text{ in } \Omega^{\mathrm{a}}. \tag{2.12}$$

Proof. Choose $\boldsymbol{u}_\Gamma \in H^{\mathrm{div}}(\Omega^{\mathrm{a}})$ such that $\boldsymbol{u}_\Gamma \cdot \boldsymbol{\nu} = u_{\boldsymbol{\nu}}(0)$ on Γ and define $\boldsymbol{u}_\Omega \in H_0^{\mathrm{div}}(\Omega^{\mathrm{a}})$ such that

$$\operatorname{div} \boldsymbol{u}_\Omega = -c^{-2}\psi^1 - \operatorname{div} \boldsymbol{u}_\Gamma.$$

Condition (2.9) ensures the existence of $\boldsymbol{u}_\Omega$, since

$$(c^{-2}\psi^1 + \operatorname{div} \boldsymbol{u}_\Gamma,\, 1)_{\Omega^{\mathrm{a}}} = (c^{-2}\psi^1, 1)_{\Omega^{\mathrm{a}}} + \langle u_{\boldsymbol{\nu}}(0), 1\rangle_\Gamma = 0.$$

In order to guarantee (2.11), we define $\zeta \in V_d$ by

$$(\mathbf{curl}\, \zeta, \mathbf{curl}\, \tau)_{\Omega^{\mathrm{a}}} = -(\boldsymbol{u}_\Gamma + \boldsymbol{u}_\Omega, \mathbf{curl}\, \tau)_{\Omega^{\mathrm{a}}}, \quad \tau \in V_d,$$

noting that the lemma of Lax–Milgram yields the unique existence of ζ. The function $\boldsymbol{u}^0 = \boldsymbol{u}_\Gamma + \boldsymbol{u}_\Omega + \mathbf{curl}\, \zeta$ then satisfies (2.10), (2.11) by construction.

For checking the uniqueness, we assume that $\boldsymbol{u}_1, \boldsymbol{u}_2 \in H^{\mathrm{div}}(\Omega^{\mathrm{a}})$ satisfy (2.10), (2.11). Then, the difference $\delta\boldsymbol{u} = \boldsymbol{u}_1 - \boldsymbol{u}_2$ is an element of $H_0^{\mathrm{div}}(\Omega^{\mathrm{a}})$, and by (2.10), we have $\operatorname{div} \delta\boldsymbol{u} = 0$. Due to (2.11), we can apply the second part of Lemma 1.1 and conclude that $\delta\boldsymbol{u} = 0$ since

$$\|\delta\boldsymbol{u}(\cdot)\|_{\mathrm{div},\Omega^{\mathrm{a}}} \sim \|\operatorname{div} \delta\boldsymbol{u}(\cdot)\|_{0,\Omega^{\mathrm{a}}} = 0.$$

Given $\psi^0 \in H^1(\Omega^{\mathrm{a}})$, it is trivial to see that (2.12) uniquely determines $\boldsymbol{u}^1 \in L^2(\Omega^{\mathrm{a}})$. □

Remark 2.5. *It is interesting to note that $\boldsymbol{u}^0$ is determined solely by ψ^1, and that $\boldsymbol{u}^1$ only depends on ψ^0. Moreover, going in the other direction and trying to construct compatible initial data for Problem 2.1 from given data for Problem 2.2 might fail. Although* (2.10) *would determine ψ^1, it is in general not possible to construct ψ^0 from* (2.12) *without additionally assuming that $\boldsymbol{u}^1$ is irrotational.*

2.4. Equivalence of the acoustic problems. LEMMA 2.6. *Let ψ be the solution of Problem 2.1, and let $\boldsymbol{u}^0$, $\boldsymbol{u}^1$ be constructed by means of Lemma 2.4. Define $\boldsymbol{u} \in L^2(H_*^{\mathrm{div}}(\Omega^{\mathrm{a}}))$ by*

$$\operatorname{div} \boldsymbol{u} = -c^{-2}\dot{\psi}, \tag{2.13a}$$

$$(\boldsymbol{u}(\cdot), \mathbf{curl}\, \tau)_{\Omega^{\mathrm{a}}} = 0, \qquad \tau \in V_d. \tag{2.13b}$$

Then, the function $\boldsymbol{u}$

i) is uniquely defined by (2.13),

ii) satisfies

$$\dot{\boldsymbol{u}} = -\operatorname{grad} \psi, \tag{2.14}$$

iii) is the unique solution of Problem 2.2 with initial data $\boldsymbol{u}^0$, $\boldsymbol{u}^1$.

Proof. We note that (2.13) has the same structure as (2.10), (2.11). In order to prove i), it is sufficient to show that the compatibility between $\dot{\psi}$ and $u_{\boldsymbol{\nu}}$ holds. To do so, we choose $\boldsymbol{u}_\Gamma \in L^2(H_*^{\mathrm{div}}(\Omega^{\mathrm{a}}))$ and define $\boldsymbol{u}_\Omega \in L^2(H_0^{\mathrm{div}}(\Omega^{\mathrm{a}}))$ such that

$$\operatorname{div} \boldsymbol{u}_\Omega = -c^{-2}\dot{\psi} - \operatorname{div} \boldsymbol{u}_\Gamma.$$

Conditions (2.8), (2.9), the balance equation (2.3), and the fact that $\boldsymbol{u}_\Gamma \in L^2(H_*^{\mathrm{div}}(\Omega^{\mathrm{a}}))$ yield the required compatibility by observing that

$$\begin{aligned}
&\int_0^t (\operatorname{div} \boldsymbol{u}_\Gamma(s) + c^{-2}\dot{\psi}(s), 1)_{\Omega^{\mathrm{a}}} \,\mathrm{d}s \\
&\quad = \int_0^t \left(\langle u_{\boldsymbol{\nu}}(s), 1\rangle_{1/2,\Gamma} + (c^{-2}\psi^1, 1)_{\Omega^{\mathrm{a}}} + \int_0^s \langle c^{-2}\ddot{\psi}(\tau), 1\rangle_{1,\Omega^{\mathrm{a}}} \,\mathrm{d}\tau \right) \mathrm{d}s \\
&\quad = \int_0^t \left(\langle u_{\boldsymbol{\nu}}(0), 1\rangle_{1/2,\Gamma} + (c^{-2}\psi^1, 1)_{\Omega^{\mathrm{a}}} + \int_0^s \langle c^{-2}\ddot{\psi}(\tau), 1\rangle_{1,\Omega^{\mathrm{a}}} + \langle \dot{u}_{\boldsymbol{\nu}}(\tau), 1\rangle_{1/2,\Gamma} \,\mathrm{d}\tau \right) \mathrm{d}s \\
&\quad = 0.
\end{aligned}$$

We proceed by proving ii). From (2.13b), it follows that

$$(\dot{\boldsymbol{u}}(\cdot), \mathbf{curl}\, \tau)_{\Omega^{\mathrm{a}}} = 0, \qquad \tau \in V_d.$$

Thus, the first part of Lemma 1.1 can be applied yielding $\dot{\boldsymbol{u}} = \operatorname{grad} \alpha$ with $\alpha \in L^2(H^1(\Omega^{\mathrm{a}}))$. Moreover, we observe by using (2.13a), (2.8), (2.3) that for $\phi \in H^1(\Omega^{\mathrm{a}})$

$$\begin{aligned}
(\dot{\boldsymbol{u}}(\cdot) + \operatorname{grad} \psi(\cdot), \operatorname{grad} \phi)_{\Omega^{\mathrm{a}}} &= -\langle \operatorname{div} \dot{\boldsymbol{u}}(\cdot), \phi\rangle_{1,\Omega^{\mathrm{a}}} + \langle \dot{\boldsymbol{u}}(\cdot)\cdot\boldsymbol{\nu}, \phi\rangle_{1/2,\Gamma} + (\operatorname{grad} \psi(\cdot), \operatorname{grad} \phi)_{\Omega^{\mathrm{a}}} \\
&= \langle c^{-2}\ddot{\psi}(\cdot), \phi\rangle_{1,\Omega^{\mathrm{a}}} + \langle \dot{u}_{\boldsymbol{\nu}}(\cdot), \phi\rangle_{1/2,\Gamma} + (\operatorname{grad} \psi(\cdot), \operatorname{grad} \phi)_{\Omega^{\mathrm{a}}} \\
&= 0,
\end{aligned}$$

which gives (2.14).

In order to check iii), we insert $\boldsymbol{u}$ defined by (2.13) into the left hand side of (2.7), test with $\boldsymbol{v} \in H_0^{\mathrm{div}}(\Omega^{\mathrm{a}})$, and see that

$$\langle \ddot{\boldsymbol{u}}(\cdot), \boldsymbol{v}\rangle_{\mathrm{div},\Omega^{\mathrm{a}}} + (c^2 \operatorname{div} \boldsymbol{u}(\cdot), \operatorname{div} \boldsymbol{v})_{\Omega^{\mathrm{a}}} = -\langle \operatorname{grad} \dot{\psi}(\cdot), \boldsymbol{v}\rangle_{\mathrm{div},\Omega^{\mathrm{a}}} - (\dot{\psi}(\cdot), \operatorname{div} \boldsymbol{v})_{\Omega^{\mathrm{a}}} = 0.$$

Comparing (2.10)-(2.12) with (2.13)-(2.14) makes it obvious that the initial conditions (2.5) are also satisfied. $\square$

3. Discretization of the acoustic problems. This section is divided into two parts. First, Subsection 3.1 describes the standard semi- and fully discrete acoustic problems originating from the continuous ones. Second, the fully discrete problem for the acoustic displacement is modified and the equivalence of the resulting problems is shown in Subsection 3.2.

3.1. Standard discrete problem formulations. We proceed in the usual way and formulate semi-discrete problems as an intermediate step, thereby introducing the finite element spaces. After that, Newmark's time integration method is employed to derive fully discrete problems.

3.1.1. Semi-discrete problems. For the approximation of the acoustic velocity potential, we use the space S^1_{a} of globally continuous and piecewise linear finite elements with respect to a shape-regular simplicial triangulation $\mathcal{T}_{\mathrm{a}}$ of Ω^{a}, and set $S^1_{\mathrm{a},0} = S^1_{\mathrm{a}} \cap H^1_0(\Omega^{\mathrm{a}})$. Originating from an approximate solution in the solid domain, the Neumann data $v_{\boldsymbol{\nu}}$ from (2.1) is replaced by $v_{\boldsymbol{\nu},h} \in C^0(L^2(\Gamma))$. We note that our formulation admits the use of non-matching grids for the coupled elasto-acoustic problem, as will be carried out in Section 4. With Π^1_Γ denoting the L^2-projection onto piecewise linear functions with respect to the faces of $\mathcal{T}_{\mathrm{a}}$ along Γ, we arrive at the following semi-discrete problem.

Problem 3.1. *Given approximations $\psi^0_h, \psi^1_h \in S^1_{\mathrm{a}}$ of ψ^0, ψ^1, as well as $v_{\boldsymbol{\nu},h} \in C^0(L^2(\Gamma))$, seek $\psi_h \in C^0(S^1_{\mathrm{a}})$ such that for all times $t \in (0,T)$*

$$(c^{-2}\ddot{\psi}_h(t), \phi)_{\Omega^{\mathrm{a}}} + (\operatorname{grad}\psi_h(t), \operatorname{grad}\phi)_{\Omega^{\mathrm{a}}} = -(v_{\boldsymbol{\nu},h}(t), \phi)_\Gamma, \quad \phi \in S^1_{\mathrm{a}},$$

together with

$$\psi_h(0) = \psi^0_h \quad \text{and} \quad \dot{\psi}_h(0) = \psi^1_h.$$

The displacement field is discretized within the space

$$\widehat{RT}^0 = \{\boldsymbol{w} \in RT^1 : \boldsymbol{w}\cdot\boldsymbol{\nu}_f \in \mathbb{P}_{0,f}, f \in \mathcal{F}_{\mathrm{i}}\} \supset RT^0,$$

where RT^k, $k \geq 0$, denotes the standard family of H^{div}-conforming Raviart–Thomas finite element spaces, [8], $\mathbb{P}_{0,f}$ is the space of constant functions on the face f, $\boldsymbol{\nu}_f$ is a fixed unit normal on f, and $\mathcal{F}_{\mathrm{i}}$ stands for the set of all *inner* faces of $\mathcal{T}_{\mathrm{a}}$. Furthermore, we set

$$\widehat{RT}^0_0 = \{\boldsymbol{v} \in \widehat{RT}^0 : \boldsymbol{v}\cdot\boldsymbol{\nu} = 0 \text{ on } \Gamma\}.$$

In the following, we will frequently make use of the following properties of $\widehat{RT}^0$:

(P1) We have $\operatorname{div}\widehat{RT}^0_0 = \widetilde{W}^1 = \{\phi \in W^1 : (\phi,1)_{\Omega^{\mathrm{a}}} = 0\}$, and the pairing $\widehat{RT}^0_0 \times \widetilde{W}^1$ is uniformly inf-sup stable, i.e., there exists $c > 0$ such that

$$\sup_{\boldsymbol{w}\in\widehat{RT}^0_0} \frac{(\operatorname{div}\boldsymbol{w}, \phi)_{\Omega^{\mathrm{a}}}}{\|\boldsymbol{w}\|_{\mathrm{div},\Omega^{\mathrm{a}}}} \geq c\|\phi\|_0, \qquad \phi \in \widetilde{W}^1. \tag{3.1}$$

(P2) If $\boldsymbol{w} \in \widehat{RT}^0_0$ and $\operatorname{div}\boldsymbol{w} = 0$, then $\boldsymbol{w} = \mathbf{curl}\,\tau$ for $\tau \in K^1_d$, where $K^1_d = S^1_{\mathrm{a},0}$ for $d = 2$, and K^1_d is the lowest order Nédélec space with one degree of freedom per inner edge for $d = 3$.

(P3) If $\boldsymbol{w} \in \widehat{RT}^0_0$ and $(\boldsymbol{w}, \mathbf{curl}\,\tau)_{\Omega^{\mathrm{a}}} = 0$ for all $\tau \in K^1_d$, then $\|\boldsymbol{w}\|_{\mathrm{div},\Omega^{\mathrm{a}}} \leq C\|\operatorname{div}\boldsymbol{w}\|_{0,\Omega^{\mathrm{a}}}$.

We note that (P1) and (P2) can be shown by straightforward calculations, using the inf-sup stability of the standard pairing $RT^1_0 \times \widetilde{W}^1$ and discrete norm equivalences, [27, (B.35)]. Then, the theory of saddle point problems yields the equivalence of (3.1) and (P3), see [7, Lemma III.4.2].

Since the essential data $u_{\boldsymbol{\nu},h} \in C^0(L^2(\Gamma))$ provided by the solid domain has to be respected, we set

$$C^0(\widehat{RT}^0_*) = \{\boldsymbol{v} \in C^0(\widehat{RT}^0) : \boldsymbol{v}\cdot\boldsymbol{\nu} = \Pi^1_\Gamma u_{\boldsymbol{\nu},h} \text{ on } \Gamma\times(0,T)\}.$$

The semi-discrete problem for the displacement field is given as follows.

Problem 3.2. *Given approximations $\boldsymbol{u}^0_h, \boldsymbol{u}^1_h \in \widehat{RT}^0$ of $\boldsymbol{u}^0, \boldsymbol{u}^1$, as well as $u_{\boldsymbol{\nu},h} \in C^0(L^2(\Gamma))$, and provided that $\boldsymbol{u}^0_h\cdot\boldsymbol{\nu} = \Pi^1_\Gamma u_{\boldsymbol{\nu},h}(0)$, find $\boldsymbol{u}_h \in C^0(\widehat{RT}^0_*)$ such that for all times $t \in (0,T)$*

$$(\ddot{\boldsymbol{u}}_h(t), \boldsymbol{v})_{\Omega^{\mathrm{a}}} + (c^2\operatorname{div}\boldsymbol{u}_h(t), \operatorname{div}\boldsymbol{v})_{\Omega^{\mathrm{a}}} = 0, \qquad \boldsymbol{v} \in \widehat{RT}^0_0,$$

together with

$$\boldsymbol{u}_h(0) = \boldsymbol{u}^0_h \quad \text{and} \quad \dot{\boldsymbol{u}}_h(0) = \boldsymbol{u}^1_h.$$

Given ψ_h^0 and ψ_h^1, we would like to specify $\boldsymbol{u}_h^0$ and $\boldsymbol{u}_h^1$ such that a discrete analog of (2.10)-(2.12) holds. Our choice of the space $\widehat{RT}^0$ is motivated by the observation that the first equation of (2.10) can be satisfied in a strong form. We stress the fact that $S_{\mathrm{a}}^1 \subset \operatorname{div} \widehat{RT}^0 = \operatorname{div} RT^1$, but $S_{\mathrm{a}}^1 \not\subset \operatorname{div} RT^0$. However, (2.12) cannot be satisfied in general, since $\operatorname{grad} S_{\mathrm{a}}^1 \not\subset H^{\operatorname{div}}(\Omega^{\mathrm{a}})$. This reason prevents an equivalence of Problems 3.1 and 3.2 by means of (2.13a), (2.14). We therefore postpone this issue until Section 3.2.

3.1.2. Fully discrete problems. Starting from the semi-discrete Problems 3.1 and 3.2, one can employ a suitable time integration scheme, as for example Newmark's method, [13, 19]. In particular, we decompose the interval $[0, T]$ into subintervals $[t_n, t_{n+1}]$, $n = 0, \ldots, N_t - 1$, with $t_n = n\Delta t$, $\Delta t = T/N_t$. For a time-dependent quantity x, we denote by $x_n \approx x(t_n)$ its approximation at $t = t_n$. The characteristic feature of the classical Newmark method is to compute the approximations $\dot{x}_{n+1}$ and $\ddot{x}_{n+1}$ as functions of x_{n+1} and the already known values $x_n, \dot{x}_n, \ddot{x}_n$,

$$\dot{x}_{n+1} = 2\Delta t^{-1}(x_{n+1} - x_n) - \dot{x}_n, \tag{3.2a}$$

$$\ddot{x}_{n+1} = 4\Delta t^{-2}(x_{n+1} - x_n) - 4\Delta t^{-1}\dot{x}_n - \ddot{x}_n. \tag{3.2b}$$

It is well known that the classical Newmark scheme is unconditionally stable and of quadratic order with respect to time.

Assuming that the boundary data is now given by sequences $u_{\boldsymbol{\nu},n}, v_{\boldsymbol{\nu},n} \in L^2(\Gamma)$, and setting

$$\widehat{RT}^0_{*,n} = \{\boldsymbol{v} \in \widehat{RT}^0 : \boldsymbol{v} \cdot \boldsymbol{\nu} = \Pi_\Gamma^1 u_{\boldsymbol{\nu},n} \text{ on } \Gamma\},$$

the fully discrete problems are stated as follows.

PROBLEM 3.3. *Given approximations $\psi_h^0, \psi_h^1 \in S_{\mathrm{a}}^1$ of ψ^0, ψ^1, as well as boundary data $v_{\boldsymbol{\nu},n} \in L^2(\Gamma)$, find sequences $\psi_n, \dot{\psi}_n, \ddot{\psi}_n \in S_{\mathrm{a}}^1$ such that for $n = 0, \ldots, N_t$*

$$(c^{-2}\ddot{\psi}_n, \phi)_{\Omega^{\mathrm{a}}} + (\operatorname{grad}\psi_n, \operatorname{grad}\phi)_{\Omega^{\mathrm{a}}} = -(v_{\boldsymbol{\nu},n}, \phi)_\Gamma, \quad \phi \in S_{\mathrm{a}}^1, \tag{3.3}$$

together with (3.2) *and*

$$\psi_0 = \psi_h^0 \quad \textit{and} \quad \dot{\psi}_0 = \psi_h^1.$$

PROBLEM 3.4. *Given approximations $\boldsymbol{u}_h^0 \in \widehat{RT}^0_{*,0}$ and $\boldsymbol{u}_h^1 \in \widehat{RT}^0$ of $\boldsymbol{u}^0$ and $\boldsymbol{u}^1$, respectively, and boundary data $u_{\boldsymbol{\nu},n} \in L^2(\Gamma)$, find sequences $\boldsymbol{u}_n \in \widehat{RT}^0_{*,n}$ and $\dot{\boldsymbol{u}}_n, \ddot{\boldsymbol{u}}_n \in \widehat{RT}^0$ such that for $n = 0, \ldots, N_t$*

$$(\ddot{\boldsymbol{u}}_n, \boldsymbol{v})_{\Omega^{\mathrm{a}}} + (c^2 \operatorname{div}\boldsymbol{u}_n, \operatorname{div}\boldsymbol{v})_{\Omega^{\mathrm{a}}} = 0, \qquad \boldsymbol{v} \in \widehat{RT}^0_0, \tag{3.4}$$

together with (3.2) *and*

$$\boldsymbol{u}_0 = \boldsymbol{u}_h^0 \quad \textit{and} \quad \dot{\boldsymbol{u}}_0 = \boldsymbol{u}_h^1.$$

REMARK 3.5. *For the classical Newmark scheme, Problem 3.4 is equivalent to the "acoustic part" of Algorithm 1 from [3], and only the result of a different notation which is more suitable for our upcoming investigations. In particular, in [3], the velocities and accelerations are eliminated by obtaining from* (3.2)

$$\begin{aligned}
x_1 - x_0 - \Delta t\dot{x}_0 &= \frac{\Delta t^2}{4}(\ddot{x}_1 + \ddot{x}_0),\\
x_{n+1} - 2x_n + x_{n-1} &= (x_{n+1} - x_n) - (x_n - x_{n-1})\\
&= \Delta t\dot{x}_n + \frac{\Delta t^2}{4}(\ddot{x}_{n+1} + \ddot{x}_n) - \Delta t\dot{x}_{n-1} - \frac{\Delta t^2}{4}(\ddot{x}_n + \ddot{x}_{n-1})\\
&= \Delta t(\dot{x}_n - \dot{x}_{n-1}) + \frac{\Delta t^2}{4}(\ddot{x}_{n+1} - \ddot{x}_{n-1})\\
&= \frac{\Delta t^2}{4}(\ddot{x}_{n+1} + 2\ddot{x}_n + \ddot{x}_{n-1}),
\end{aligned}$$

which allows to modify (3.4) *to*

$$\Delta t^{-2}((\boldsymbol{u}_1 - \boldsymbol{u}_0 - \Delta t \boldsymbol{u}_h^1), \boldsymbol{v})_{\Omega^{\mathrm{a}}} + \frac{1}{4}(c^2 \operatorname{div}(\boldsymbol{u}_0 + \boldsymbol{u}_1), \operatorname{div} \boldsymbol{v})_{\Omega^{\mathrm{a}}} = 0,$$

to find the first iterate $\boldsymbol{u}_1$*, and to*

$$\Delta t^{-2}((\boldsymbol{u}_{n+1} - 2\boldsymbol{u}_n + \boldsymbol{u}_{n-1}), \boldsymbol{v})_{\Omega^{\mathrm{a}}} + \frac{1}{4}(c^2 \operatorname{div}(\boldsymbol{u}_{n+1} + 2\boldsymbol{u}_n + \boldsymbol{u}_{n-1}), \operatorname{div} \boldsymbol{v})_{\Omega^{\mathrm{a}}} = 0,$$

for $n \geq 1$*, which is exactly the form found in [3]. Thus, we are able to use the stability anaylsis from there. Since our main emphasis is to establish explicit relations between* $\psi_n, \dot{\psi}_n, \ddot{\psi}_n$ *and* $\boldsymbol{u}_n, \dot{\boldsymbol{u}}_n, \ddot{\boldsymbol{u}}_n$*, we prefer the notation of Problems 3.3 and 3.4.*

3.2. Equivalent discrete problem formulations. In the following, we discuss the modification which is necessary to formulate equivalent discrete problems, introduce discrete compatibility conditions, and actually show the equivalence.

3.2.1. Projection and problem modification. We define $\widetilde{\Pi}^0$ as the projection $L^2(\Omega^{\mathrm{a}}) \to \widetilde{\mathbb{P}}_0 = \operatorname{grad} S_{\mathrm{a}}^1/\mathbb{P}_0 + \mathbf{curl}\, K_d^1$, and modify Problem 3.4 to:

PROBLEM 3.6. *Given approximations* $\boldsymbol{u}_h^0 \in \widehat{RT}^0_{*,0}$ *and* $\boldsymbol{u}_h^1 \in \widehat{RT}^0$ *of* $\boldsymbol{u}^0$ *and* $\boldsymbol{u}^1$*, respectively, and boundary data* $u_{\boldsymbol{\nu},n} \in L^2(\Gamma)$*, find sequences* $\boldsymbol{w}_n \in \widehat{RT}^0_{*,n}$*,* $\dot{\boldsymbol{w}}_n \in \widehat{RT}^0$*, and* $\widetilde{\Pi}^0 \ddot{\boldsymbol{w}}_n \in \widetilde{\mathbb{P}}_0$ *such that for* $n = 0, \dots, N_t$

$$(\widetilde{\Pi}^0 \ddot{\boldsymbol{w}}_n, \boldsymbol{v})_{\Omega^{\mathrm{a}}} + (c^2 \operatorname{div} \boldsymbol{w}_n, \operatorname{div} \boldsymbol{v})_{\Omega^{\mathrm{a}}} = 0, \qquad \boldsymbol{v} \in \widehat{RT}^0_0, \tag{3.5}$$

together with (3.2) *and*

$$\boldsymbol{w}_0 = \boldsymbol{u}_h^0 \quad \textit{and} \quad \dot{\boldsymbol{w}}_0 = \boldsymbol{u}_h^1.$$

REMARK 3.7. *It is not necessary to explicitly construct a sequence* $\ddot{\boldsymbol{w}}_n \in \widehat{RT}^0$*. It is sufficient to deal with* $\widetilde{\Pi}^0 \ddot{\boldsymbol{w}}_n \in \widetilde{\mathbb{P}}_0$*, where the expression* $\widetilde{\Pi}^0 \ddot{\boldsymbol{w}}_n$ *is interpreted as one single symbol, rather than as the application of the operator* $\widetilde{\Pi}^0$ *to* $\ddot{\boldsymbol{w}}_n$*. As we will see later, the choice of* $\boldsymbol{w}_0$ *guarantees that* $\widetilde{\Pi}^0 \ddot{\boldsymbol{w}}_0$ *is well defined.*

3.2.2. Discrete compatibility conditions.

Boundary data. We have to modify the compatibility of the boundary data (2.8) to account for the fully discrete setting. To this end, we assume that the two sequences $u_{\boldsymbol{\nu},n}$, $v_{\boldsymbol{\nu},n} \in L^2(\Gamma)$ are related in the sense of (3.2a) by

$$v_{\boldsymbol{\nu},n+1} = 2\Delta t^{-1}(u_{\boldsymbol{\nu},n+1} - u_{\boldsymbol{\nu},n}) - v_{\boldsymbol{\nu},n}. \tag{3.6}$$

For the coupled elasto-acoustic problem, we will see in Section 4 that (3.6) is automatically satisfied if the same Newmark scheme is used on both subdomains.

Initial data. The projection $\widetilde{\Pi}^0$ admits to formulate a discrete analog of Lemma 2.4.

LEMMA 3.8. *Let the initial and boundary data* ψ_h^0*,* ψ_h^1*, and* $v_{\boldsymbol{\nu},n}$ *of Problem 3.3 be given. Let also the boundary data* $u_{\boldsymbol{\nu},n}$ *of Problem 3.6 satisfying* (3.6) *be given and assume additionally that*

$$-(c^{-2}\psi_h^1, 1)_{\Omega^{\mathrm{a}}} = (u_{\boldsymbol{\nu},0}, 1)_{\Gamma}. \tag{3.7}$$

Then, initial data $\boldsymbol{u}_h^0$*,* $\boldsymbol{u}_h^1$ *of Problem 3.6 can be selected such that*

$$\operatorname{div} \boldsymbol{u}_h^0 = -c^{-2}\psi_h^1, \tag{3.8}$$

$$\widetilde{\Pi}^0 \boldsymbol{u}_h^1 = -\operatorname{grad} \psi_h^0. \tag{3.9}$$

Proof. Given $\psi^1 \in S_{\mathrm{a}}^1$, condition (3.7) and Property (P1) guarantees the existence of $\boldsymbol{u}_h^0 \in \widehat{RT}^0_{*,0}$ satisfying (3.8).

We determine $\boldsymbol{u}_h^1$ as a solution of

$$(\operatorname{div} \boldsymbol{u}_h^1, \phi)_{\Omega^{\mathrm{a}}} = (\operatorname{grad} \psi_h^0, \operatorname{grad} \phi)_{\Omega^{\mathrm{a}}} + (v_{\boldsymbol{\nu},0}, \phi)_\Gamma, \ \phi \in S_{\mathrm{a}}^1, \quad \boldsymbol{u}_h^1 \cdot \boldsymbol{\nu} = \Pi_\Gamma^1 v_{\boldsymbol{\nu},0} \text{ on } \Gamma, \tag{3.10}$$

$$(\boldsymbol{u}_h^1, \operatorname{\mathbf{curl}} \tau)_{\Omega^{\mathrm{a}}} = 0, \quad \tau \in K_d^1. \tag{3.11}$$

We observe that (3.10) is solvable for $\boldsymbol{u}_h^1 \in \widehat{RT}^0$, since $S_{\mathrm{a}}^1 \subset W^1$ and

$$(\operatorname{div} \boldsymbol{u}_h^1, 1)_{\Omega^{\mathrm{a}}} - (\operatorname{grad} \psi_h^0, \operatorname{grad} 1)_{\Omega^{\mathrm{a}}} - (\Pi_\Gamma^1 v_{\boldsymbol{\nu},0}, 1)_\Gamma = (\boldsymbol{u}_h^1 \cdot \boldsymbol{\nu}, 1)_\Gamma - (\Pi_\Gamma^1 v_{\boldsymbol{\nu},0}, 1)_\Gamma = 0.$$

We can additionally require (3.11) without violating (3.10). Note that $\boldsymbol{u}_h^1$ is not uniquely determined by (3.10)-(3.11). Nevertheless, we can show (3.9) by first testing with $\operatorname{\mathbf{curl}} \tau$, $\tau \in K_d^1$, yielding

$$(\widetilde{\Pi}^0 \boldsymbol{u}_h^1 + \operatorname{grad} \psi_h^0, \operatorname{\mathbf{curl}} \tau)_{\Omega^{\mathrm{a}}} = (\boldsymbol{u}_h^1 + \operatorname{grad} \psi_h^0, \operatorname{\mathbf{curl}} \tau)_{\Omega^{\mathrm{a}}} = 0$$

due to (3.11) and $\operatorname{\mathbf{curl}} K_d^1 \perp \operatorname{grad} S_{\mathrm{a}}^1$, and second by testing with $\operatorname{grad} \phi$, $\phi \in S_{\mathrm{a}}^1$, which gives

$$(\widetilde{\Pi}^0 \boldsymbol{u}_h^1 + \operatorname{grad} \psi_h^0, \operatorname{grad} \phi)_{\Omega^{\mathrm{a}}} = -(\operatorname{div} \boldsymbol{u}_h^1, \phi)_{\Omega^{\mathrm{a}}} + (\boldsymbol{u}_h^1 \cdot \boldsymbol{\nu}, \phi)_\Gamma + (\operatorname{grad} \psi_h^0, \operatorname{grad} \phi)_{\Omega^{\mathrm{a}}} = 0$$

due to (3.10). □

3.2.3. Discrete equivalence. We prove the equivalence of the fully discrete problems by means of the following lemma.

LEMMA 3.9. *Let $\psi_n, \dot\psi_n, \ddot\psi_n$ be the solution of Problem 3.3. For $n = 1, \ldots, N_t$, define $\boldsymbol{w}_n \in \widehat{RT}^0_{*,n}$, $\dot{\boldsymbol{w}}_n \in \widehat{RT}^0$, and $\widetilde{\Pi}^0 \ddot{\boldsymbol{w}}_n \in \widetilde{\mathbb{P}}_0$ by*

$$\operatorname{div} \boldsymbol{w}_n = -c^{-2} \dot\psi_n, \qquad \boldsymbol{w}_n \cdot \boldsymbol{\nu} = \Pi_\Gamma^1 u_{\boldsymbol{\nu},n} \text{ on } \Gamma, \tag{3.12a}$$

$$(\boldsymbol{w}_n, \operatorname{\mathbf{curl}} \tau)_{\Omega^{\mathrm{a}}} = 0, \quad \tau \in K_d^1, \tag{3.12b}$$

together with (3.2)*. For $n = 0$, choose the initial data $\boldsymbol{w}_0 = \boldsymbol{u}_h^0$ and $\dot{\boldsymbol{w}}_0 = \boldsymbol{u}_h^1$ according to Lemma 3.8, and obtain $\widetilde{\Pi}^0 \ddot{\boldsymbol{w}}_0$ by* (3.5)*. Then, the sequences $\boldsymbol{w}_n, \dot{\boldsymbol{w}}_n, \widetilde{\Pi}^0 \ddot{\boldsymbol{w}}_n$*

i) are uniquely defined for $n \geq 1$ by (3.12) *and* (3.2)*.*

ii) satisfy

$$\widetilde{\Pi}^0 \dot{\boldsymbol{w}}_n = -\operatorname{grad} \psi_n, \tag{3.13}$$

iii) are the solution of Problem 3.6 with initial data $\boldsymbol{w}_0, \dot{\boldsymbol{w}}_0$.

Proof. The discrete compatibility conditions (3.6), (3.7) yield the existence of $\boldsymbol{w}_n$ satisfying (3.12), while (P3) guarantees the uniqueness.

Relation (3.12a) is immediately obvious from Lemma 3.8 for n=0 and from (3.12a) for $n \geq 1$. We give a proof by induction for (3.13) and the supplementary results

$$(a)\ \dot{\boldsymbol{w}}_n \cdot \boldsymbol{\nu} = \Pi_\Gamma^1 v_{\boldsymbol{\nu},n}, \quad (b)\ (\operatorname{div} \dot{\boldsymbol{w}}_n, \phi)_{\Omega^{\mathrm{a}}} = -(c^{-2} \ddot\psi_n, \phi)_{\Omega^{\mathrm{a}}}, \ \phi \in S_{\mathrm{a}}^1, \quad (c)\ \widetilde{\Pi}^0 \ddot{\boldsymbol{w}}_n = -\operatorname{grad} \dot\psi_n. \tag{3.14}$$

For $n = 0$, (3.13) and (3.14a) follow from Lemma 3.8, while (3.14b) can be derived by choosing $\phi \in S_{\mathrm{a}}^1$, and using (3.3) in combination with Lemma 3.8,

$$\begin{aligned} (c^{-2} \ddot\psi_0, \phi)_{\Omega^{\mathrm{a}}} &= -(\operatorname{grad} \psi_0, \operatorname{grad} \phi)_{\Omega^{\mathrm{a}}} - (v_{\boldsymbol{\nu},0}, \phi)_\Gamma = (\widetilde{\Pi}^0 \dot{\boldsymbol{w}}_0, \operatorname{grad} \phi)_{\Omega^{\mathrm{a}}} - (v_{\boldsymbol{\nu},0}, \phi)_\Gamma \\ &= (\dot{\boldsymbol{w}}_0, \operatorname{grad} \phi)_{\Omega^{\mathrm{a}}} - (v_{\boldsymbol{\nu},0}, \phi)_\Gamma = -(\operatorname{div} \dot{\boldsymbol{w}}_0, \phi)_{\Omega^{\mathrm{a}}}. \end{aligned}$$

Similarly, taking $\boldsymbol{v} \in \widehat{RT}_0^0$, (3.14c) is obtained from (3.5),

$$\begin{aligned} (\widetilde{\Pi}^0 \ddot{\boldsymbol{w}}_0, \boldsymbol{v})_{\Omega^{\mathrm{a}}} &= -(c^2 \operatorname{div} \boldsymbol{w}_0, \operatorname{div} \boldsymbol{v})_{\Omega^{\mathrm{a}}} = (\dot\psi_0, \operatorname{div} \boldsymbol{v})_{\Omega^{\mathrm{a}}} \\ &= (\dot\psi_0, \operatorname{div} \boldsymbol{v})_{\Omega^{\mathrm{a}}} = -(\operatorname{grad} \dot\psi_0, \boldsymbol{v})_{\Omega^{\mathrm{a}}}. \end{aligned}$$

Assume now (3.13)-(3.14) with n replaced by $n-1$. Employing (3.2a), the induction assumption, the fact that $\boldsymbol{w}_n \in \widehat{RT}^0_{*,n}$, and (3.6), we obtain (3.14a) by

$$\begin{aligned}\dot{\boldsymbol{w}}_n \cdot \boldsymbol{\nu} &= 2/\Delta t(\boldsymbol{w}_n \cdot \boldsymbol{\nu} - \boldsymbol{w}_{n-1} \cdot \boldsymbol{\nu}) - \dot{\boldsymbol{w}}_{n-1} \cdot \boldsymbol{\nu} \\ &= 2/\Delta t(\Pi^1_\Gamma u_{\boldsymbol{\nu},n} - \Pi^1_\Gamma u_{\boldsymbol{\nu},n-1}) - \Pi^1_\Gamma v_{\boldsymbol{\nu},n-1} = \Pi^1_\Gamma v_{\boldsymbol{\nu},n}.\end{aligned}$$

In the same way, using the induction assumption and (3.2), we obtain (3.14b) by

$$\begin{aligned}(\operatorname{div} \dot{\boldsymbol{w}}_n, \phi)_{\Omega^{\mathrm{a}}} &= (2/\Delta t(\operatorname{div} \boldsymbol{w}_n - \operatorname{div} \boldsymbol{w}_{n-1}) - \operatorname{div} \dot{\boldsymbol{w}}_{n-1},\ \phi)_{\Omega^{\mathrm{a}}} \\ &= (2/\Delta t(-c^{-2}\dot{\psi}_n + c^{-2}\dot{\psi}_{n-1}) + c^{-2}\ddot{\psi}_{n-1},\ \phi)_{\Omega^{\mathrm{a}}} = -(c^{-2}\ddot{\psi}_n, \phi)_{\Omega^{\mathrm{a}}}.\end{aligned}$$

The definition of $\widetilde{\Pi}^0$ and (3.12b) yield $\widetilde{\Pi}^0 \boldsymbol{w}_n = \operatorname{grad} \alpha$ with $\alpha \in S^1_{\mathrm{a}}$. Via (3.2a), we immediately obtain $\widetilde{\Pi}^0 \dot{\boldsymbol{w}}_n = \operatorname{grad} \dot{\alpha}_h$ for a function $\dot{\alpha}_h \in S^1_{\mathrm{a}}$. Moreover, we observe by (3.3) together with the fact that $\Pi^1_\Gamma \phi_h = \phi_h$ for $\phi_h \in S^1_{\mathrm{a}}$ on Γ, and by (3.14a), (3.14b), that

$$\begin{aligned}(\widetilde{\Pi}^0 \dot{\boldsymbol{w}}_n + \operatorname{grad} \psi_n, \operatorname{grad} \phi_h)_{\Omega^{\mathrm{a}}} &= (\dot{\boldsymbol{w}}_n + \operatorname{grad} \psi_n, \operatorname{grad} \phi_h)_{\Omega^{\mathrm{a}}} \\ &= -(\operatorname{div} \dot{\boldsymbol{w}}_n, \phi_h)_{\Omega^{\mathrm{a}}} + (v_{\boldsymbol{\nu},n}, \phi_h)_\Gamma + (\operatorname{grad} \psi_n, \operatorname{grad} \phi_h)_{\Omega^{\mathrm{a}}} \\ &= (c^{-2}\ddot{\psi}_n, \phi_h)_{\Omega^{\mathrm{a}}} + (v_{\boldsymbol{\nu},n}, \phi_h)_\Gamma + (\operatorname{grad} \psi_n, \operatorname{grad} \phi_h)_{\Omega^{\mathrm{a}}} = 0,\end{aligned}$$

which gives (3.13). Relation (3.2) immediately yields (3.14c), which concludes the induction proof.

In order to check iii), we insert $\boldsymbol{w}_n$ defined by (3.12) and $\widetilde{\Pi}^0 \ddot{\boldsymbol{w}}_n$ defined by (3.2) into the left side of (3.5), test with $\boldsymbol{v}_h \in \widehat{RT}^0_0$, use (3.14c), (3.12a), and see that

$$(\widetilde{\Pi}^0 \ddot{\boldsymbol{w}}_n, \boldsymbol{v}_h)_{\Omega^{\mathrm{a}}} + (c^2 \operatorname{div} \boldsymbol{w}_n, \operatorname{div} \boldsymbol{v}_h)_{\Omega^{\mathrm{a}}} = -(\operatorname{grad} \dot{\psi}_n, \boldsymbol{v}_h)_{\Omega^{\mathrm{a}}} - (\dot{\psi}_n, \operatorname{div} \boldsymbol{v}_h)_{\Omega^{\mathrm{a}}} = 0,$$

which concludes the proof of this lemma. □

Remark 3.10. *If additionally* $\operatorname{div} \dot{\boldsymbol{w}}_0 = -c^{-2}\ddot{\psi}_0$*, then (3.14b) holds for all n in a strong sense. We note that this can be easily guaranteed by replacing* (3.10) *with*

$$\operatorname{div} \boldsymbol{u}^1_h = -c^{-2}\ddot{\psi}_0, \qquad \boldsymbol{u}^1_h \cdot \boldsymbol{\nu} = \Pi^1_\Gamma v_{\boldsymbol{\nu},0},$$

where $\ddot{\psi}_0 \in S^1_{\mathrm{a}}$ is defined by (3.3)*. Then, $\boldsymbol{u}^1_h$ is uniquely defined and* (3.10) *also holds. Moreover, we note that Π^1_Γ only enters the definition of the displacement based formulation and not Problem 3.3. In the case of matching meshes, Π^1_Γ does not enter at all if piecewise linear finite elements are used for the elasticity problem.*

3.3. A priori analysis of the discretization error in space. The difference between the original discrete Problem 3.4 and its modification 3.6 is only in the inertia terms. Quite often, the discretization of the inertia term can be simplified by applying inexact quadrature formulas, [2]. This process is well known from the parabolic case, where it is also referred to as mass lumping. The influence of this variational crime can be analyzed in terms of the approximation properties of an associated oprator, i.e., the use of the projection $\widetilde{\Pi}^0$ can be interpreted as employing a mass lumping process. In contrast to standard mass lumping, the resulting mass matrix is singular, and $\widetilde{\Pi}^0$ is a global operator. We note that recently in [12], the corresponding effect has been rigorously investigated for a linear elasticity problem with a singular mass matrix. As it turns out, the crucial ingredient for the analysis of the time-discrete problem is the quality of suitable associated elliptic stationary problems: Find $\boldsymbol{y} \in H^{\operatorname{div}}(\Omega^{\mathrm{a}})$ with given normal components $y_{\boldsymbol{\nu}}$ on the boundary and $\boldsymbol{y}_h \in \widehat{RT}^0_0$ with $\Pi^1_\Gamma y_{\boldsymbol{\nu}}$ as boundary condition such that

$$\begin{aligned} a(\boldsymbol{y}, \boldsymbol{v}) &= (\boldsymbol{b}, \boldsymbol{v})_{\Omega^{\mathrm{a}}}, \quad \boldsymbol{v} \in H^{\operatorname{div}}_0(\Omega^{\mathrm{a}}), \\ a_h(\boldsymbol{y}_h, \boldsymbol{v}) &= (\boldsymbol{b}, \boldsymbol{v})_{\Omega^{\mathrm{a}}}, \quad \boldsymbol{v} \in \widehat{RT}^0_0,\end{aligned}$$

where $\boldsymbol{b} \in L^2(\Omega^{\mathrm{a}})$ with $(\boldsymbol{b}, \operatorname{\mathbf{curl}} \tau)_{0,\Omega^{\mathrm{a}}} = 0$ for $\tau \in V_d$ and

$$\begin{aligned} a_h(\boldsymbol{v}, \boldsymbol{w}) &= (\omega \widetilde{\Pi}^0 \boldsymbol{v}, \boldsymbol{w})_{\Omega^{\mathrm{a}}} + (\operatorname{div} \boldsymbol{v}, \operatorname{div} \boldsymbol{w})_{\Omega^{\mathrm{a}}} \quad \boldsymbol{v}, \boldsymbol{w} \in H^{\operatorname{div}}(\Omega^{\mathrm{a}}), \\ a(\boldsymbol{v}, \boldsymbol{w}) &= (\omega \boldsymbol{v}, \boldsymbol{w})_{\Omega^{\mathrm{a}}} + (\operatorname{div} \boldsymbol{v}, \operatorname{div} \boldsymbol{w})_{\Omega^{\mathrm{a}}} \quad \boldsymbol{v}, \boldsymbol{w} \in H^{\operatorname{div}}(\Omega^{\mathrm{a}}),\end{aligned}$$

with $\omega > 0$.

As a preliminary result for the analysis of the discretization error $\boldsymbol{y}-\boldsymbol{y}_h$, we state the following lemma.

LEMMA 3.11. *The bilinear form $a_h(\cdot,\cdot)$ is $\widehat{RT}_0^0$-elliptic.* **Proof.** We write $\boldsymbol{v} \in \widehat{RT}_0^0$ as $\boldsymbol{v} = \boldsymbol{v}_0 + \boldsymbol{v}_\perp$ such that $\operatorname{div} \boldsymbol{v}_0 = 0$ and that $(\boldsymbol{v}_\perp, \mathbf{curl}\,\tau)_{\Omega^{\mathrm{a}}} = 0$ for all $\tau \in K_d^1$. From (P2), it follows that $\boldsymbol{v}_0 = \mathbf{curl}\,\tau$ with $\tau \in K_d^1$, which immediately implies

$$\widetilde{\Pi}^0 \boldsymbol{v}_0 = \boldsymbol{v}_0. \tag{3.15}$$

We have that

$$(\widetilde{\Pi}^0 \boldsymbol{v}_0, \widetilde{\Pi}^0 \boldsymbol{v}_\perp)_{\Omega^{\mathrm{a}}} = (\widetilde{\Pi}^0 \boldsymbol{v}_0, \boldsymbol{v}_\perp)_{\Omega^{\mathrm{a}}} = (\boldsymbol{v}_0, \boldsymbol{v}_\perp)_{\Omega^{\mathrm{a}}} = 0,$$

which gives

$$\|\widetilde{\Pi}^0 \boldsymbol{v}\|_{0,\Omega^{\mathrm{a}}}^2 = \|\widetilde{\Pi}^0 \boldsymbol{v}_0\|_{0,\Omega^{\mathrm{a}}}^2 + \|\widetilde{\Pi}^0 \boldsymbol{v}_\perp\|_{0,\Omega^{\mathrm{a}}}^2 \geq \|\widetilde{\Pi}^0 \boldsymbol{v}_0\|_{0,\Omega^{\mathrm{a}}}^2.$$

Starting with $\|\boldsymbol{v}\|_{\mathrm{div},\Omega^{\mathrm{a}}}^2 = \|\boldsymbol{v}_0\|_{0,\Omega^{\mathrm{a}}}^2 + \|\boldsymbol{v}_\perp\|_{\mathrm{div},\Omega^{\mathrm{a}}}^2$ and using (P3), we obtain

$$\begin{aligned}\|\boldsymbol{v}\|_{\mathrm{div},\Omega^{\mathrm{a}}}^2 &\leq \|\boldsymbol{v}_0\|_{0,\Omega^{\mathrm{a}}}^2 + C\|\operatorname{div} \boldsymbol{v}_\perp\|_{0,\Omega^{\mathrm{a}}}^2 = \|\widetilde{\Pi}^0 \boldsymbol{v}_0\|_{0,\Omega^{\mathrm{a}}}^2 + C\|\operatorname{div} \boldsymbol{v}_\perp\|_{0,\Omega^{\mathrm{a}}}^2 \\ &\leq \|\widetilde{\Pi}^0 \boldsymbol{v}\|_{0,\Omega^{\mathrm{a}}}^2 + C\|\operatorname{div} \boldsymbol{v}\|_{0,\Omega^{\mathrm{a}}}^2 \leq C a_h(\boldsymbol{v},\boldsymbol{v}),\end{aligned}$$

which concludes the proof. □

REMARK 3.12. *For the coercivity of $a_h(\cdot,\cdot)$, it would be sufficient to set $\widetilde{\Pi}^0$ to the projection onto $\mathbf{curl}\,K_d^1$ instead of the more complex one onto $\mathbf{curl}\,K_d^1 + \operatorname{grad} S_{\mathrm{a}}^1$. However, this choice could not lead to optimal a priori estimates, as will be shown in the next theorem.*

THEOREM 3.13. *Under the assumption that $\boldsymbol{y} \in H^1(\Omega^{\mathrm{a}})$ and $\operatorname{div} \boldsymbol{y} \in H^1(\Omega^{\mathrm{a}})$, we find*

$$\|\boldsymbol{y} - \boldsymbol{y}_h\|_{\mathrm{div},\Omega^{\mathrm{a}}} \leq Ch.$$

Proof. By means of Lemma 1.1, the assumption on $\boldsymbol{b}$ guarantees that $\boldsymbol{y} = \operatorname{grad} \xi$ with $\xi \in \widetilde{H}^1(\Omega^{\mathrm{a}})$. Now, we define $\xi_h \in S_{\mathrm{a}}^1/\mathbb{P}_0$ uniquely by

$$(\operatorname{grad} \xi_h, \operatorname{grad} \phi)_{\Omega^{\mathrm{a}}} = -(\operatorname{div} \boldsymbol{y}, \phi)_{\Omega^{\mathrm{a}}} + (y_{\boldsymbol{\nu}}, \phi)_\Gamma, \quad \phi \in S_{\mathrm{a}}^1$$

and note that the right hand side is compatible. We thus observe that ξ_h is the conforming finite element solution of a Neumann problem, and that a standard a priori estimate holds, i.e.,

$$\|\operatorname{grad} \xi_h - \operatorname{grad} \xi\|_{0,\Omega^{\mathrm{a}}} \leq Ch.$$

Additionally, we set $\boldsymbol{v}_h \in \widehat{RT}^0$ such that $\boldsymbol{v}_h \cdot \boldsymbol{\nu} = \Pi_\Gamma^1 y_{\boldsymbol{\nu}}$ and

$$\begin{aligned}(\operatorname{div} \boldsymbol{v}_h, w)_{\Omega^{\mathrm{a}}} &= (\operatorname{div} \boldsymbol{y}, w)_{\Omega^{\mathrm{a}}}, \quad w \in \widetilde{W}^1, \\ (\boldsymbol{v}_h, \mathbf{curl}\,\tau)_{\Omega^{\mathrm{a}}} &= 0, \quad \tau \in K_d^1.\end{aligned}$$

We note that by definition, $\operatorname{div} \boldsymbol{v}_h = \operatorname{div} \widehat{\Pi}_{\mathrm{F}}^0 \boldsymbol{y}$ and $\boldsymbol{v}_h \cdot \boldsymbol{\nu} = \widehat{\Pi}_{\mathrm{F}}^0 \boldsymbol{y} \cdot \boldsymbol{\nu}$, where $\widehat{\Pi}_{\mathrm{F}}^0$ stands for the Fortin operator on $\widehat{RT}^0$, see, e.g., [8]. Thus, we have $\boldsymbol{v}_h - \widehat{\Pi}_{\mathrm{F}}^0 \boldsymbol{y} = \mathbf{curl}\,\tau \in \mathbf{curl}\,K_d^1$ yielding

$$\begin{aligned}\|\boldsymbol{v}_h - \widehat{\Pi}_{\mathrm{F}}^0 \boldsymbol{y}\|_{\mathrm{div},\Omega^{\mathrm{a}}}^2 =& \|\boldsymbol{v}_h - \widehat{\Pi}_{\mathrm{F}}^0 \boldsymbol{y}\|_{0,\Omega^{\mathrm{a}}}^2 = (\boldsymbol{v}_h - \widehat{\Pi}_{\mathrm{F}}^0 \boldsymbol{y}, \mathbf{curl}\,\tau)_{\Omega^{\mathrm{a}}} \\ =& (\boldsymbol{y} - \widehat{\Pi}_{\mathrm{F}}^0 \boldsymbol{y}, \mathbf{curl}\,\tau)_{\Omega^{\mathrm{a}}} \leq \|\boldsymbol{y} - \widehat{\Pi}_{\mathrm{F}}^0 \boldsymbol{y}\|_{0,\Omega^{\mathrm{a}}} \|\boldsymbol{v}_h - \widehat{\Pi}_{\mathrm{F}}^0 \boldsymbol{y}\|_{0,\Omega^{\mathrm{a}}},\end{aligned}$$

and thus the triangle inequality gives

$$\|\boldsymbol{v}_h - \boldsymbol{y}\|_{\mathrm{div},\Omega^{\mathrm{a}}} \leq 2\|\boldsymbol{y} - \widehat{\Pi}_{\mathrm{F}}^0 \boldsymbol{y}\|_{\mathrm{div},\Omega^{\mathrm{a}}} \leq Ch.$$

Moreover, following the same lines as in the proof of Lemma 3.8, we find $\widetilde{\Pi}^0 \boldsymbol{v}_h = \operatorname{grad} \xi_h$. Note that by definition, we have $\boldsymbol{v}_h - \boldsymbol{y}_h \in \widehat{RT}_0^0$. Using the triangle inequality, we obtain in terms of Lemma 3.11

$$\|\boldsymbol{y} - \boldsymbol{y}_h\|^2_{\operatorname{div},\Omega^{\mathrm{a}}} \leq C(\|\boldsymbol{y} - \boldsymbol{v}_h\|^2_{\operatorname{div},\Omega^{\mathrm{a}}} + a_h(\boldsymbol{y}_h - \boldsymbol{v}_h, \boldsymbol{y}_h - \boldsymbol{v}_h)),$$

and the definition of the bilinear forms and of $\boldsymbol{v}_h$ yield

$$\begin{aligned} a_h(\boldsymbol{y}_h - \boldsymbol{v}_h, \boldsymbol{y}_h - \boldsymbol{v}_h) &= a(\boldsymbol{y}, \boldsymbol{y}_h - \boldsymbol{v}_h) - (\omega \operatorname{grad} \xi_h, \boldsymbol{y}_h - \boldsymbol{v}_h)_{\Omega^{\mathrm{a}}} - (\operatorname{div} \boldsymbol{y}, \operatorname{div}(\boldsymbol{y}_h - \boldsymbol{v}_h))_{\Omega^{\mathrm{a}}} \\ &= (\omega(\operatorname{grad} \xi - \operatorname{grad} \xi_h), \boldsymbol{y}_h - \boldsymbol{v}_h)_{\Omega^{\mathrm{a}}} \\ &\leq C\| \operatorname{grad} \xi - \operatorname{grad} \xi_h\|_{\Omega^{\mathrm{a}}} \|\boldsymbol{y}_h - \boldsymbol{v}_h\|_{\Omega^{\mathrm{a}}} \end{aligned}$$

and thus

$$a_h(\boldsymbol{y}_h - \boldsymbol{v}_h, \boldsymbol{y}_h - \boldsymbol{v}_h) \leq C\| \operatorname{grad} \xi - \operatorname{grad} \xi_h\|^2_{\Omega^{\mathrm{a}}}.$$

Therefore, we have $\|\boldsymbol{y} - \boldsymbol{y}_h\|_{\operatorname{div},\Omega^{\mathrm{a}}} \leq C(\|\boldsymbol{y} - \boldsymbol{v}_h\|_{\operatorname{div},\Omega^{\mathrm{a}}} + \| \operatorname{grad} \xi - \operatorname{grad} \xi_h\|_{0,\Omega^{\mathrm{a}}}) \leq Ch.$ □

4. Coupled elasto-acoustic problems.

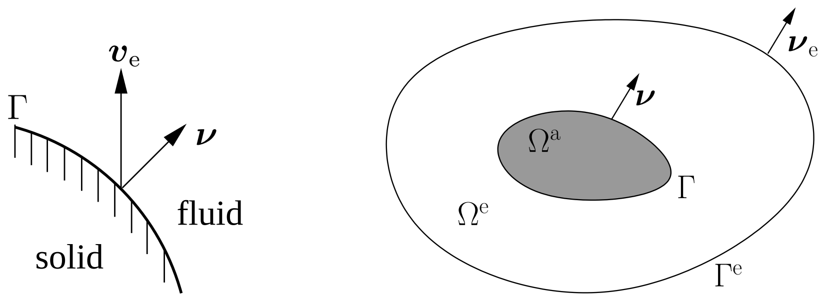

FIGURE 4.1. *Left: solid-fluid interface, right: setup of the coupled elasto-acoustic problem.*

4.1. The elasticity problem. Assuming small deformations, small strain, and no volume forces, it is sufficient to investigate the linear system

$$\rho_{\mathrm{e}} \ddot{\boldsymbol{u}}_{\mathrm{e}} - \operatorname{div}(\sigma(\boldsymbol{u}_{\mathrm{e}})) = 0 \quad \text{in } \Omega^{\mathrm{e}} \times (0,T), \tag{4.1}$$

with the linearized stress tensor σ given by Hooke's Law

$$\sigma = \lambda_{\mathrm{L}}(\operatorname{tr} \varepsilon)\mathrm{Id} + 2\mu_{\mathrm{L}}\, \varepsilon, \tag{4.2}$$

with the Lamé constants $\lambda_{\mathrm{L}}, \mu_{\mathrm{L}}$, and with the linearized strain tensor

$$\varepsilon(\boldsymbol{u}) = \frac{1}{2}(\operatorname{grad} \boldsymbol{u} + [\operatorname{grad} \boldsymbol{u}]^{\mathrm{t}}), \tag{4.3}$$

complemented by the interface condition (4.9) introduced below, the boundary conditions

$$\begin{aligned} \boldsymbol{u}_{\mathrm{e}} = \boldsymbol{0} \quad &\text{on } \Gamma^{\mathrm{e}}_{\mathrm{D}} \times (0,T), \\ \sigma(\boldsymbol{u}_{\mathrm{e}})\boldsymbol{\nu}_{\mathrm{e}} = \boldsymbol{g}_{\mathrm{e}} \quad &\text{on } \Gamma^{\mathrm{e}}_{\mathrm{N}} \times (0,T), \end{aligned}$$

and initial conditions

$$\boldsymbol{u}_{\mathrm{e}}(0) = \boldsymbol{u}^0_{\mathrm{e}} \quad \text{and} \quad \dot{\boldsymbol{u}}_{\mathrm{e}}(0) = \boldsymbol{u}^1_{\mathrm{e}} \quad \text{in } \Omega^{\mathrm{e}}. \tag{4.4}$$

The surface traction $\boldsymbol{g}_\Gamma$ acting on the fluid-structure interface Γ represents the coupling of forces between Ω^{e} and Ω^{a}. Transforming to the weak form, and defining the space

$$H^1_*(\Omega^{\mathrm{e}}) = \{\boldsymbol{v} \in H^1(\Omega^{\mathrm{e}}) : \boldsymbol{v} = 0 \text{ on } \Gamma^{\mathrm{e}}_{\mathrm{D}}\},$$

we obtain for the mechanical system the following problem.

Problem 4.1. *Given* $\boldsymbol{u}_{\mathrm{e}}^0 \in H_*^1(\Omega^{\mathrm{e}})$, $\boldsymbol{u}_{\mathrm{e}}^1 \in L^2(\Omega^{\mathrm{e}})$, $\boldsymbol{g}_{\mathrm{e}} \in L^2(H^{-1/2}(\Gamma_N^{\mathrm{e}}))$, *and* $\boldsymbol{g}_\Gamma \in L^2(H^{-1/2}(\Gamma))$, *find a displacement field* $\boldsymbol{u}_{\mathrm{e}} \in L^2(H_*^1(\Omega^{\mathrm{e}}))$ *such that for all times* $t \in (0,T)$

$$\langle \rho_e \ddot{\boldsymbol{u}}_{\mathrm{e}}(t),\, \boldsymbol{v}\rangle_{1,\Omega^{\mathrm{e}}} + (\sigma(\boldsymbol{u}_{\mathrm{e}}(t)),\, \varepsilon(\boldsymbol{v}))_{\Omega^{\mathrm{e}}} - \langle \boldsymbol{g}_\Gamma(t), \boldsymbol{v}\rangle_{1/2,\Gamma} = \langle \boldsymbol{g}_e(t), \boldsymbol{v}\rangle_{1/2,\Gamma_N^{\mathrm{e}}}, \quad \boldsymbol{v} \in H_*^1(\Omega^{\mathrm{e}}),$$

together with the initial conditions (4.4).

For the approximation of the elastic displacements, we use the space S_{e}^1 of vector-valued globally continuous and piecewise linear finite elements with respect to a shape-regular simplicial triangulation $\mathcal{T}_{\mathrm{e}}$ of Ω^{e}, and set $S_{\mathrm{e},*}^1 = S_{\mathrm{e}}^1 \cap H_*^1(\Omega^{\mathrm{e}})$. Using the same time integration scheme as for the acoustic part, we arrive at the following fully discrete elasticity problem.

Problem 4.2. *Given approximations* $\boldsymbol{u}_{\mathrm{e},h}^0 \in S_{\mathrm{e},*}^1$ *and* $\boldsymbol{u}_{\mathrm{e},h}^1 \in S_{\mathrm{e}}^1$ *of* $\boldsymbol{u}_{\mathrm{e}}^0$ *and* $\boldsymbol{u}_{\mathrm{e}}^1$, *respectively, and boundary data* $\boldsymbol{g}_{\Gamma,n} \in L^2(\Gamma)$, *find sequences* $\boldsymbol{u}_{\mathrm{e},n} \in S_{\mathrm{e},*}^1$ *and* $\dot{\boldsymbol{u}}_{\mathrm{e},n}, \ddot{\boldsymbol{u}}_{\mathrm{e},n} \in S_{\mathrm{e}}^1$ *such that for* $n = 0,\ldots,N_t$

$$(\rho_e \ddot{\boldsymbol{u}}_{\mathrm{e},n}, \boldsymbol{v})_{\Omega^{\mathrm{e}}} + (\sigma(\boldsymbol{u}_{\mathrm{e},n}),\, \varepsilon(\boldsymbol{v}))_{\Omega^{\mathrm{e}}} - (\boldsymbol{g}_{\Gamma,n}, \boldsymbol{v})_\Gamma = (\boldsymbol{g}_{\mathrm{e},n}, \boldsymbol{v})_\Gamma, \qquad \boldsymbol{v} \in S_{\mathrm{e},*}^1, \tag{4.5}$$

together with (3.2) *and*

$$\boldsymbol{u}_{\mathrm{e},0} = \boldsymbol{u}_{\mathrm{e},h}^0 \quad \textit{and} \quad \dot{\boldsymbol{u}}_{\mathrm{e},0} = \boldsymbol{u}_{\mathrm{e},h}^1.$$

4.2. Interface conditions. At the solid-fluid interface Γ, as depicted in Figure 4.1, the continuity requires that the normal component of the mechanical surface velocity of the solid must coincide with the normal component of the acoustic velocity of the fluid. Thus, the following relation between the velocity $\boldsymbol{v}_{\mathrm{e}} = \dot{\boldsymbol{u}}_{\mathrm{e}}$ of the solid expressed by the mechanical displacement $\boldsymbol{u}_{\mathrm{e}}$ and the acoustic particle velocity $\boldsymbol{v}_{\mathrm{a}}$ arises:

$$\boldsymbol{v}_{\mathrm{a}} \cdot \boldsymbol{\nu} = \dot{\boldsymbol{u}}_{\mathrm{e}} \cdot \boldsymbol{\nu} = \dot{u}_{\boldsymbol{\nu}}, \qquad \text{on } \Gamma \ \times \ (0,T), \tag{4.6}$$

where the unit normal vector field $\boldsymbol{\nu}$ on Γ points outward of Ω^{a}. Moreover, we assume that the initial solutions are compatible, namely,

$$\boldsymbol{u}_{\mathrm{a},0} \cdot \boldsymbol{\nu} = \boldsymbol{u}_{\mathrm{e},0} \cdot \boldsymbol{\nu}, \qquad \text{on } \Gamma. \tag{4.7}$$

Given this compatibility, we can equivalently describe (4.6) by requiring the continuity of the displacements, i.e.,

$$\boldsymbol{u}_{\mathrm{a}} \cdot \boldsymbol{\nu} = \boldsymbol{u}_{\mathrm{e}} \cdot \boldsymbol{\nu} = u_{\boldsymbol{\nu}}, \qquad \text{on } \Gamma \ \times \ (0,T). \tag{4.8}$$

In addition to (4.6) or (4.8), one has to consider the fact that the ambient fluid causes a surface force $\boldsymbol{g}_\Gamma$ which acts like a pressure load on the solid. Therefore, a second coupling condition is given by

$$\sigma(\boldsymbol{u}_{\mathrm{e}})\boldsymbol{\nu} = \boldsymbol{g}_\Gamma, \qquad \text{on } \Gamma \times \ (0,T). \tag{4.9}$$

Throughout the paper, we assume that the surface force $\boldsymbol{g}_\Gamma$ only acts in normal direction. In particular, we have that

$$\boldsymbol{g}_\Gamma = c^2(\operatorname{div} \boldsymbol{u}_{\mathrm{a}})\boldsymbol{\nu} = \dot{\psi}\boldsymbol{\nu}, \qquad \text{on } \Gamma \times \ (0,T).$$

4.3. Coupled problem formulations.

4.3.1. Continuous Setting. The fully coupled potential-based elasto-acoustic problem is obtained by Problems 2.1 and 4.1 requiring that $\dot{u}_{\boldsymbol{\nu}} = \dot{\boldsymbol{u}}_{\mathrm{e}} \cdot \boldsymbol{\nu}$ and $\boldsymbol{g}_\Gamma = \dot{\psi}\boldsymbol{\nu}$. The fully coupled displacement-based elasto-acoustic problem is obtained by Problems 2.2 and 4.1 requiring $u_{\boldsymbol{\nu}} = \boldsymbol{u}_{\mathrm{e}} \cdot \boldsymbol{\nu}$ and $\boldsymbol{g}_\Gamma = c^2(\operatorname{div} \boldsymbol{u})\boldsymbol{\nu}$.

4.3.2. Discretization. The discrete coupled potential-based elasto-acoustic problem is obtained by Problems 3.3 and 4.2 requiring that $\dot{u}_{\boldsymbol{\nu},n} = \dot{\boldsymbol{u}}_{\mathrm{e},n} \cdot \boldsymbol{\nu}$ and $\boldsymbol{g}_{\Gamma,n} = \dot{\psi}_n \boldsymbol{\nu}$. The discrete coupled displacement-based elasto-acoustic problem is obtained by Problems 3.4 and 4.2 requiring $u_{\boldsymbol{\nu},n} = \boldsymbol{u}_{\mathrm{e},n} \cdot \boldsymbol{\nu}$ and $\boldsymbol{g}_{\Gamma,n} = c^2(\operatorname{div} \boldsymbol{u}_n)\boldsymbol{\nu}$.

REMARK 4.3. *The two triangulations $\mathcal{T}_{\mathrm{a}}$ and $\mathcal{T}_{\mathrm{e}}$ inherit two $(d-1)$-dimensional grids $\mathcal{T}^{\mathrm{a}}$ and $\mathcal{T}^{\mathrm{e}}$ on Γ. Due to the flexible construction of both grids, the finite element nodes on $\mathcal{T}^{\mathrm{a}}$ and $\mathcal{T}^{\mathrm{e}}$ will in general not coincide. On the contrary, motivated by different spatial scales required for the resolution of the local subproblems, the difference in the mesh sizes can become quite large.*

The discretized version of (3.3), (4.5) reads in matrix form

$$\begin{pmatrix} M_{\mathrm{a}} & 0 \\ 0 & M_{\mathrm{e}} \end{pmatrix} \begin{pmatrix} \ddot{\psi}_n \\ \ddot{\boldsymbol{u}}_{\mathrm{e},n} \end{pmatrix} + \begin{pmatrix} 0 & C_{\mathrm{ea}}^{\mathrm{T}} \\ -C_{\mathrm{ea}} & 0 \end{pmatrix} \begin{pmatrix} \dot{\psi}_n \\ \dot{\boldsymbol{u}}_{\mathrm{e},n} \end{pmatrix} + \begin{pmatrix} K_{\mathrm{a}} & 0 \\ 0 & K_{\mathrm{e}} \end{pmatrix} \begin{pmatrix} \psi_n \\ \boldsymbol{u}_{\mathrm{e},n} \end{pmatrix} = \begin{pmatrix} 0 \\ \boldsymbol{f}_n \end{pmatrix}. \tag{4.10}$$

The block diagonal entries $M_{\mathrm{e}}, M_{\mathrm{a}}, K_{\mathrm{e}}, K_{\mathrm{a}}$ can be assembled locally without needing to transfer any information across the interface. The coupling between the two grids is represented by the matrices $C_{\mathrm{ea}}^{\mathrm{T}}$ and C_{ea} which realize the boundary integrals on Γ in (3.3) and (4.5). Their entries are given by

$$C_{\mathrm{ea}} = [C_{pq}]; \quad C_{pq} = \int_{\Gamma_h^{\mathrm{a}}} \rho_{\mathrm{a}}\, \phi_p^{\mathrm{e}} \phi_q^{\mathrm{a}} \boldsymbol{\nu}\, \mathrm{d}\Gamma \;\in \mathbb{R}^d, \tag{4.11}$$

where ϕ_p^{e} is the scalar basis function associated with the node p on $\mathcal{T}^{\mathrm{e}}$, and ϕ_q^{a} is the one for node q on $\mathcal{T}^{\mathrm{a}}$. Thus, the same assembly procedures as in the case of the mortar coupling can be used, [4, 5]. It should be emphasized that the coupled system of equations remains symmetric. This is not the case if instead of the acoustic velocity potential an acoustic pressure formulation is used.

Due to the equivalence of the acoustic subproblems, it seems quite obvious that the fully coupled global problems are also equivalent. The stability results provided by [3] for the displacement-based formulation can thus be transferred to the potential-based formulation employed here. However, we will not attempt to rigorously analyze the global equivalence within this paper.

5. Numerical results. We present three numerical tests and potential applications for the elasto-acoustic coupling. In each time step, the resulting linear system is solved exactly. Since we do not have any moving bodies involved, the system matrix which has to be inverted is the same in each time step. Thus, it is possible to factor this system matrix only once, and then to reuse the factorization in each step. In the first and second test, we demonstrate the gain in flexibility for the nonconforming approach. The first example investigates an electrodynamic loudspeaker where the computation can be restricted to 2D due to symmetry. For the second test, we consider the emission of acoustic waves from several cylindrical structures. The third test is dedicated to the simulation of a piezo-electric loudspeaker where the diplacements in the structure additionally couple with the electric potential. We remark that in [11], several simpler examples are presented which compare our nonconforming approach to the traditional one using matching interface grids.

5.1. Electrodynamic Loudspeaker. Electrodynamic loudspeakers like the one depicted in Fig. 5.1 are mainly used in cars. Manufacturers of such systems face the challenge to design such loudspeakers, e.g. according to changing geometries or material properties, in the interior of cars. To avoid the costly process of building prototypes, conducting measurements and redesigning, the use of flexible CAE tools is of major importance for the reduction of costs during the development phase of a new product.

For the design of electrodynamic loudspeakers the frequency dependency of the axial pressure at 1 m distance and the electric impedance of the voice coil are the two most important parameters. Now, one can perform a harmonic analysis for each frequency of interest or perform a transient analysis using a short excitation pulse, compute the acoustic pressure at 1 m distance and divide the Fourier transformation of the pressure by the Fourier transformation of the normalized excitation pulse. Since in practice the pressure response as well as electric impedance has to be computed for a wide frequency range, the second option is preferred. It is well known from the theory of

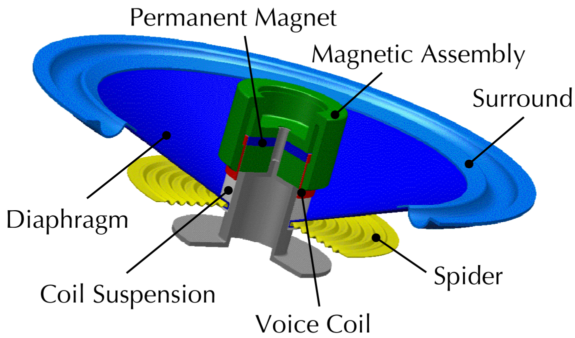

FIGURE 5.1. *Schematic of an electrodynamic loudspeaker with low construction depth (i.e. magnetic assembly in front of membrane; radius = 11.2cm, depth = 4.7cm).*

Fourier transformation, that the number of frequency samples equals the number of time samples. Therewith, to obtain a good frequency resolution, we have to perform enough time steps.

The main problem for analyzing a fully elasto-acoustic coupled model of such loudspeakers is the fact, that the mechanical subsystem consists of very thin parts like the membrane, the spider and the surround with dimensions in the thickness direction in the sub-millimeter range. The considered loudspeaker model is however designed as a subwoofer system with a maximum frequency of 5 kHz. This corresponds to a minimal acoustic wave length in air ($c = 340\,\mathrm{m/s}$) of 6.8 cm, which is about half of the radius of the speaker. It is already clear from these simple geometric arguments that the discretization in the acoustic subdomain has to be chosen much coarser than in the mechanical subdomain. As already mentioned before, the standard finite element method requires the elements to be geometrically conforming. This means for our example that the fine discretization in the mechanical subdomains has to be continued also to the acoustic far field domain, which introduces many unnecessary degrees of freedom (DOFs). This fact is demonstrated in Fig. 5.2(a)

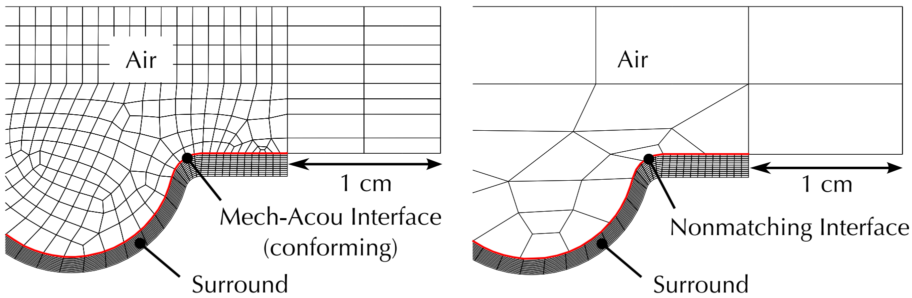

(a) Conforming (b) Non-matching

FIGURE 5.2. *Finite Element discretization in the vicinity of the surround*

The non-matching grid technique provides an excellent framework to cope with this problem since one can switch the resolution of the finite element discretization from mechanical to acoustic subdomains. This is depicted for our application in Fig. 5.2(b).

To demonstrate the advantages of the non-matching grid approach we conduct a transient simulation for the electrodynamic loudspeaker as shown in Fig. 5.1. Due to rotational symmetry, we perform an axisymmetric computation, and restrict ourself to the mechanical-acoustic coupling. Therewith, we excite the loudspeaker by applying a mechanical pressure on the top of the coil suspension in downward direction. For a fully magnetic-mechanical-acoustic coupled computation on conforming grids we refer to [22]. The excitation signal for the mechanical pressure consists of a triangular spike pulse with a duration of 60 µs. Therewith, this time signal contains a frequency band up to 5 kHz. Furthermore, the speaker is mechanically fixed at the surround as well as at the spider, and everything else may move freely. We apply absorbing boundary conditions on the outer boundary of the acoustic domain to account for free radiation. Choosing a time step size of 5μs, and computing 5000 time steps results in a frequency resolution Δf of about 40 Hz. In the reference configuration the speaker is discretized by second order Lagrangian finite elements with a minimal edge length $h_{\mathrm{m}} = 50\mu\mathrm{m}$. The acoustic far field region is also discretized with second order elements exhibiting a edge length of about $h_{\mathrm{a}} = 5\,\mathrm{mm}$, which corresponds to about 24 DOFs per wave length at 5 kHz. Therewith, the mesh results in 465, 934 acoustic DOFs and 20, 168 mechanical DOFs in our square domain with edge length of 1.8 m. The simulation took 2785 seconds measured on a 2.2 GHz Intel Core2 (Merom) dual core machine with optimized code (Intel C++ 10.1) and the direct solver Pardiso from Intel MKL 10.1 [24]. In the non-matching case we keep the discretization for the loudspeaker as in the conforming case (20.168 mechanical DOFs) but we apply a much coarser discretization for the acoustic domain ($h_{\mathrm{a}} = 10\,\mathrm{mm}$; 12 DOFs per wave length at 5 kHz). Therefore we can reduce the number of unknowns to 101.520 DOFs while still maintaining a fairly good coincidence of the signal in the point of interest with the reference signal as can bee seen from Fig. 5.3. The overall simulation time reduces to 722 seconds on the previously mentioned machine.

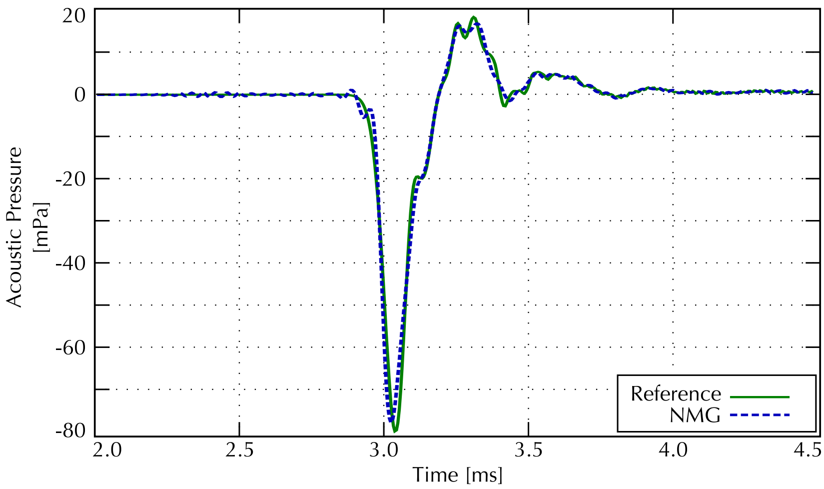

FIGURE 5.3. *Acoustic pressure signals for conforming (Reference) and non-matching grid (NMG) in point of interest (rotational axis z=1m).*

5.2. Excitation by Multiple Structures. We present the emission of acoustic waves by multiple structures which admits the steering of the waves by exciting the structures in a specified chronological order. In particular, we use for the structure Ω^{e} 25 cylindrical silicon chips with diameter 50 μm and height 1 μm. They are placed as a (5×5)-array, each plate having a distance of 50 μm to its nearest neighbors. An excitation force with frequency $f = 1\,\mathrm{MHz}$ is applied on their lower end. For the acoustic domain Ω^{a} which is assumed to be water, a cuboid of length and width 1200 μm and height 420 μm is chosen. Due to symmetry reasons, we use as computational domain one quarter of the original one. In Fig. 5.4, a part of the finite element meshes is shown, for which a uniform grid of 40×40×28 cubes is used to discretize the acoustic domain and a grid of 768 hexahedrons is employed for each full cylindrical chip. Thus, having a meshwidth of $h_{\mathrm{a}} = 600\,\mu\mathrm{m}/40 = 15\,\mu\mathrm{m}$, we use $c/(fh_{\mathrm{a}}) = 1500\mathrm{m\,s}^{-1}/(1\,\mathrm{MHz}{\cdot}h_{\mathrm{a}}) = 10$ elements per wavelength for Ω^{a}. If one had to employ matching grids, it would be quite difficult to generate them, and if the mesh-width could not be very small over the whole domain, the resulting element shapes would possibly result in a poor approximation of the solution. The nonconforming approach admits to use the grid desired for each subdomain regardless of the grids for the other subdomains. Moreover, it is very easy to add more plates or to change their position. Only the corresponding part of the coupling matrix would have to be (re-)calculated. Figures 5.5 and 5.6 show snapshots, taken every 10 time steps of 3.5 ns, of the evolution of the acoustic velocity potential ψ along with

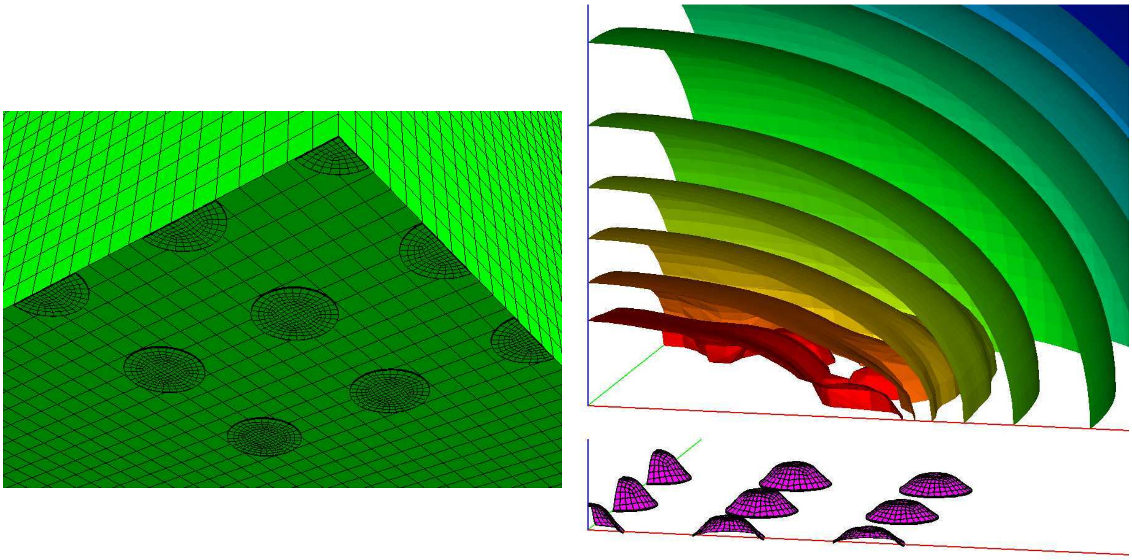

FIGURE 5.4. *Left: cylindrical plates attached to the fluid domain, right: isosurfaces of the acoustic potential, deformed plates*

the deformation of the structures (magnified by a factor of 1000). For the results presented in Figure 5.5, the cylindrical plates are excited simultaneously, while for Figure 5.6, they are excited successively. For both calculations, the waves emitting from the structures add up as expected to constitute the superposed global sound beam. Given a target point, it is possible to optimally steer the acoustic wave towards this point by appropriately adjusting the chronological order of excitation of the silicon chips. This principle is used in so-called capacitive micro-machined ultrasound transducers (CMUTs), [15]. There, the deformation of the structure is induced by an electrostatic surface force acting on the boundary. We will address a similar electric-mechanical-acoustic system in the next example by means of a piezo-electric structure, where a volume coupling of the electric and the mechanical field is considered via the constitutive law.

5.3. A Piezo-electric Loudspeaker. In our last example, we choose a piezo-electric material for a part Ω^{p} of the structure Ω^{e}, where mechanical quantities interact with an electric field. The new additional unknowns, namely, the electric potential φ, the flux density $\boldsymbol{d}$, and the electric field $\boldsymbol{e}$, correspond to the displacement $\boldsymbol{u}_{\mathrm{p}}$, the stress σ_{p}, and the strain ε_{p}, respectively. While the evolution of the mechanical displacement $\boldsymbol{u}_{\mathrm{p}}$ is still governed by the equilibrium of forces (4.1), we have to satisfy a second partial differential equation realizing the conservation of electric charge. Moreover, the coupling between the electric and the mechanical part takes place within the constitutive relations and is characterized by the elastic stiffness tensor $\mathcal{C}$, the piezo-electric tensor $\mathcal{B}$, and the dielectric permittivity tensor $\mathcal{E}$. Overall, the following coupled problem formulation is obtained: Find $(\boldsymbol{u}_{\mathrm{p}}, \varphi) : \Omega^{\mathrm{p}} \times (0,T) \to \mathbb{R}^{d+1}$ such that

$$\begin{aligned} \rho_{\mathrm{p}}\ddot{\boldsymbol{u}}_{\mathrm{p}} - \operatorname{div}\sigma_{\mathrm{p}}(\boldsymbol{u}_{\mathrm{p}},\varphi) &= \boldsymbol{f}_{\mathrm{p}}, \\ \operatorname{div}\boldsymbol{d}(\boldsymbol{u}_{\mathrm{p}},\varphi) &= q, \\ \sigma_{\mathrm{p}}(\boldsymbol{u}_{\mathrm{p}},\varphi) &= \mathcal{C}\varepsilon_{\mathrm{p}}(\boldsymbol{u}_{\mathrm{p}}) + \mathcal{B}^{\mathrm{T}}\operatorname{grad}\varphi, \\ \boldsymbol{d}(\boldsymbol{u}_{\mathrm{p}},\varphi) &= \mathcal{B}\varepsilon_{\mathrm{p}}(\boldsymbol{u}_{\mathrm{p}}) - \mathcal{E}\operatorname{grad}\varphi, \end{aligned}$$

where the strain $\varepsilon_{\mathrm{p}}(\boldsymbol{u}_{\mathrm{p}})$ is given by (4.3), complemented by appropriate boundary and initial conditions, [1]. The piezo-electric part Ω^{p} is attached to an aluminum part Ω^{q} such that $\overline{\Omega^{\mathrm{e}}} = \overline{\Omega^{\mathrm{p}} \cup \Omega^{\mathrm{q}}}$, as depicted in Figure 5.7. For Ω^{q}, we seek the displacement $\boldsymbol{u}_{\mathrm{q}}$ as solution of the standard model of linear elasto-dynamics (4.1), (4.2), and (4.3). The coupling between Ω^{p} and Ω^{q} is realized by the mortar approach, [4, 5], using dual basis functions for the approximation of the corresponding Lagrange multiplier space, [29]. For this particular example, the piezo-electric part Ω^{p} is chosen to be the lead titanate zirconate composition PZT-5 with density $\rho_{\mathrm{p}} = 7.75025{\cdot}10^3\,\mathrm{kg\,m^{-3}}$. The elastic stiffness tensor $\mathcal{C}$, the piezo-electric tensor $\mathcal{B}$, and the dielectric permittivity tensor $\mathcal{E}$ are given in Voigt notation [28] by

$$\mathcal{C} = \begin{pmatrix} c_{11} & c_{12} & c_{13} & 0 & 0 & 0 \\ c_{12} & c_{11} & c_{13} & 0 & 0 & 0 \\ c_{13} & c_{13} & c_{33} & 0 & 0 & 0 \\ 0 & 0 & 0 & c_{44} & 0 & 0 \\ 0 & 0 & 0 & 0 & c_{44} & 0 \\ 0 & 0 & 0 & 0 & 0 & (c_{11}-c_{22})/2 \end{pmatrix}, \quad \mathcal{B}^{\mathrm{T}} = \begin{pmatrix} 0 & 0 & b_{31} \\ 0 & 0 & b_{31} \\ 0 & 0 & b_{33} \\ 0 & b_{15} & 0 \\ b_{15} & 0 & 0 \\ 0 & 0 & 0 \end{pmatrix}, \quad \mathcal{E} = \begin{pmatrix} e_{11} & 0 & 0 \\ 0 & e_{11} & 0 \\ 0 & 0 & e_{33} \end{pmatrix},$$

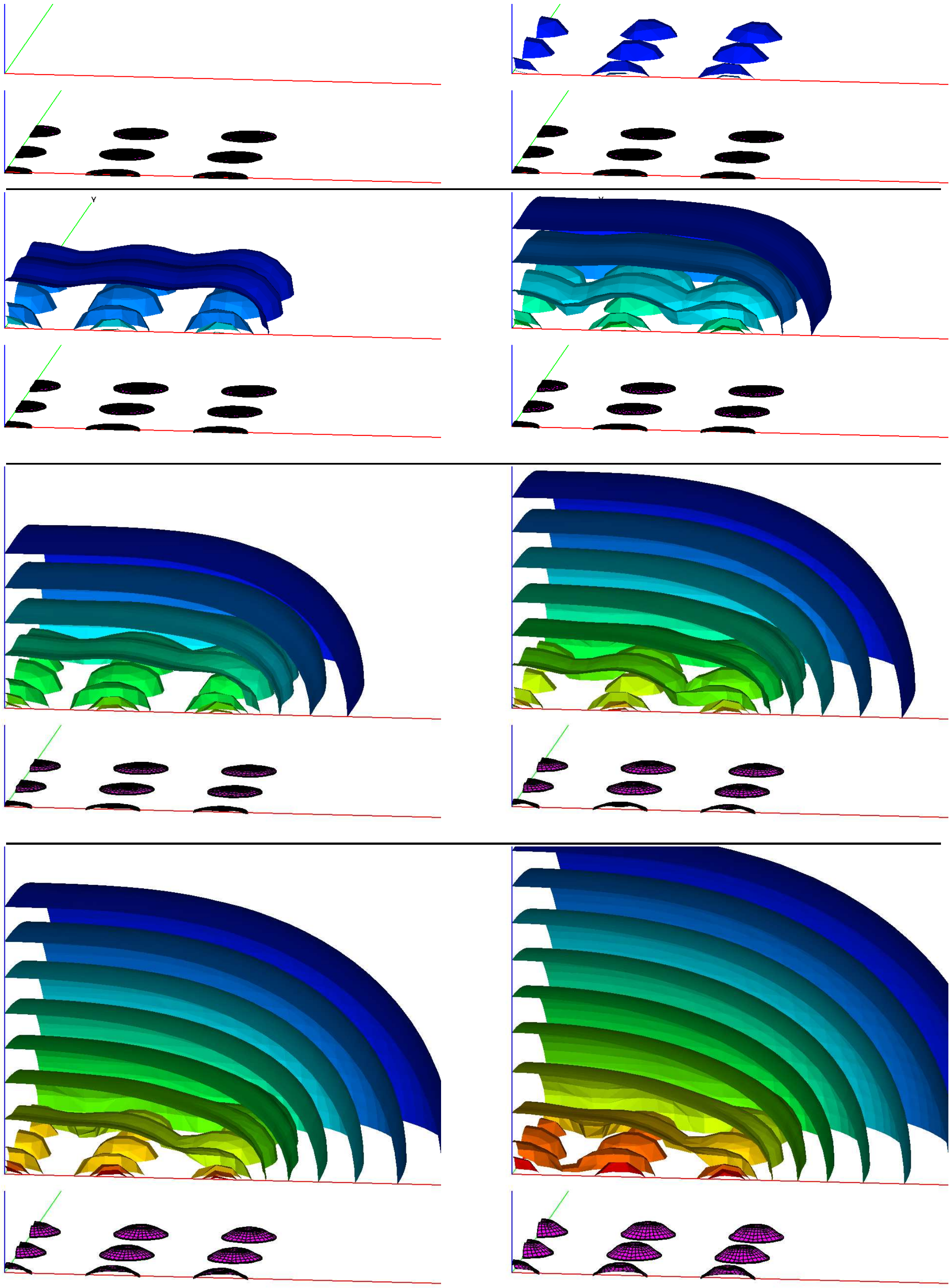

Figure 5.5. *Evolution of the acoustic velocity potential and of the deformed structures, synchronous excitation: snapshots after* $10, 20, \ldots, 80$ *timesteps.*

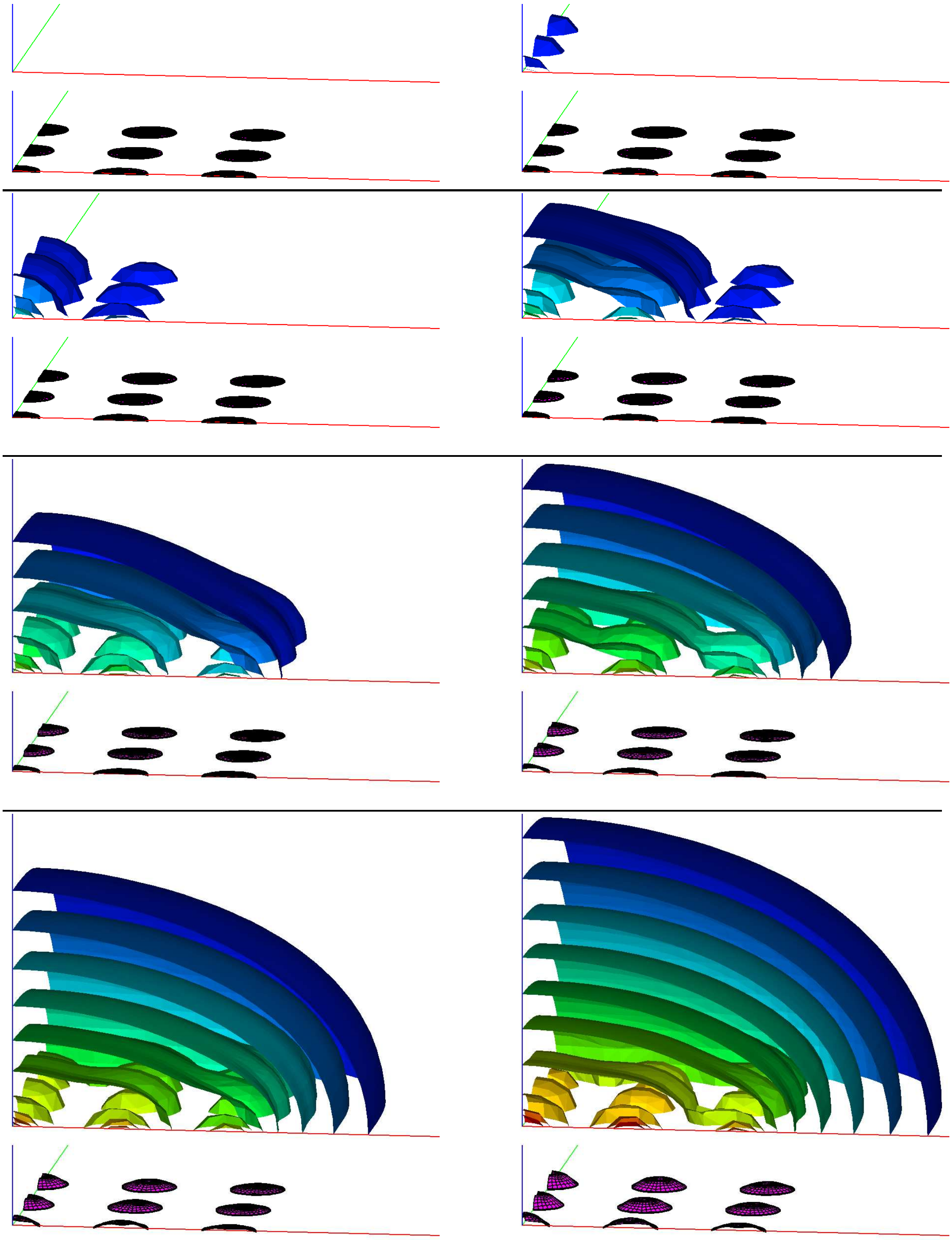

FIGURE 5.6. *Evolution of the acoustic velocity potential and of the deformed structures, successive excitation: snapshots after* $10, 20, \ldots, 80$ *timesteps.*

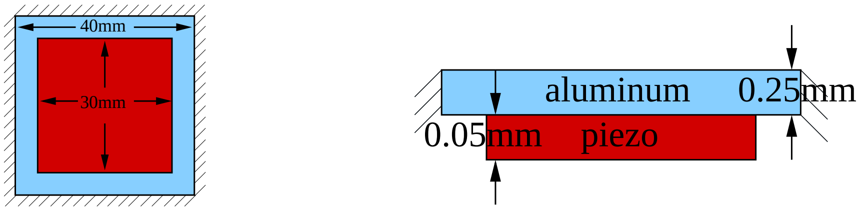

FIGURE 5.7. *Piezo-electric loudspeaker: view of the (x, y)-plane (left), (x, z)-plane (right).*

where

$$\begin{aligned}
c_{11} &= 1.26{\cdot}10^{11}\,\mathrm{N\,m^{-2}}, & c_{12} = c_{13} &= 8.41{\cdot}10^{10}\,\mathrm{N\,m^{-2}}, & c_{33} &= 1.17{\cdot}10^{11}\,\mathrm{N\,m^{-2}},\\
c_{44} &= 2.3{\cdot}10^{10}\,\mathrm{N\,m^{-2}}, & b_{31} &= -6.5\,\mathrm{C\,m^{-2}}, & b_{33} &= 23.3\,\mathrm{C\,m^{-2}},\\
b_{15} &= 17\,\mathrm{C\,m^{-2}}, & e_{11} &= 1.51{\cdot}10^{-8}\,\mathrm{C\,V^{-1}\,m^{-1}}, & e_{33} &= 1.27{\cdot}10^{-8}\,\mathrm{C\,V^{-1}\,m^{-1}}.
\end{aligned}$$

For the aluminum membrane Ω^{q}, we have the density $\rho_{\mathrm{q}} = 8.4{\cdot}10^3\,\mathrm{kg\,m^{-3}}$ and the Lamé parameters $\lambda_{\mathrm{L}} = 2.30769{\cdot}10^{10}\,\mathrm{N\,m^{-2}}$, $\mu_{\mathrm{L}} = 1.53846{\cdot}10^{10}\,\mathrm{N\,m^{-2}}$. The membrane Ω^{q} is fixed at all of its thinner sides as visualized in Figure 5.7, while the remaining boundary of the composed structure Ω^{e} remains free. Between the lower and the upper end of the piezo Ω^{p}, a potential difference $\Delta\varphi(t) = \sin 2\pi f t$ of frequency f is applied by means of a Dirichlet boundary condition for the electric potential φ.

From the geometry dimensions given in Figure 5.7, it can be seen that the ratio of length to thickness is 160 for the aluminum part Ω^{q} and 600 for the piezo-electric part Ω^{p}. From this large ratio, a strong locking effect has to be expected. We investigate this locking effect by comparing the results of the motion under a constant potential difference $\Delta\varphi = 1$ obtained by using piecewise trilinear elements with the ones from employing Serendipity elements. In order to have a more uniform element quality in terms of the ratio h/d of length to thickness, we start with $2{\times}2$ elements in Ω^{q} and $4{\times}4$ elements in Ω^{p}, and perform a uniform refinement procedure only in (x, y)-direction, thus, always using only one element in z-direction. In the left picture of Figure 5.8, the frequency of the resulting motion at the barycenter p_0 of the upper boundary of Ω^{q} is plotted, while in the right picture , the maximum vertical displacement of the same point is visualized, both times against the maximum ratio h/d of the employed elements. The results for trilinear elements clearly

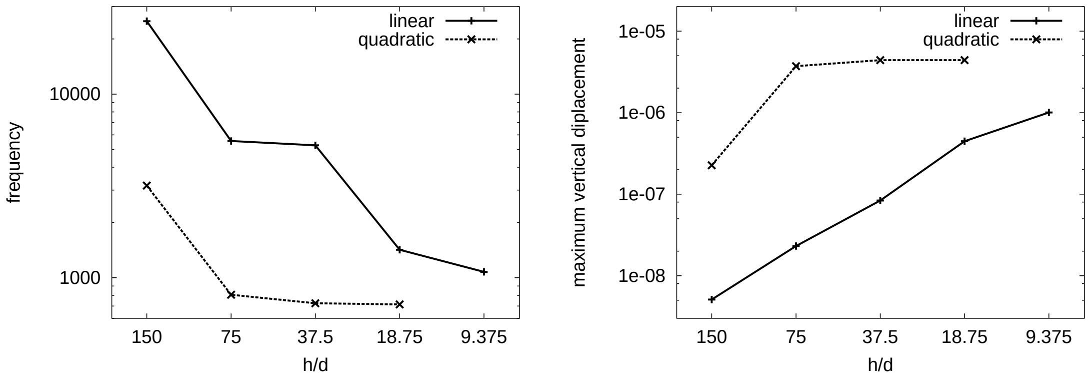

FIGURE 5.8. *Comparison of linear with quadratic elements: frequency (left), vertical displacement in p_0 (right) against the maximum ratio h/d of the elements.*

exhibit the typical signs of locking, namely, an overestimation of the frequency, an underestimation of the displacements, and a very slow convergence towards the correct values. In contrast, a rapid convergence can be observed if the quadratic Serendipity elements are used. Thus, in order to avoid locking, we discretize the structure by Serendipity elements in this example. We remark that there exist numerous alternatives for reducing locking effects for lowest order elements, [6, 25, 26].

In the following, we investigate the elastic response of the structure to applied potentials of the form $\Delta\varphi(t) = \sin(2\pi f t)$ with different frequencies f. The finite element mesh is kept fixed with $16{\times}16$ elements in Ω^{p} and $8{\times}8$ elements in Ω^{q}, corresponding to the value $h/d = 37.5$ in Figure 5.8. In particular, we examine the applicability and the effect of introducing a damping matrix C_{e} in the formulation (4.10), which should be responsible for the damping of undesired eigenmodes. We use the easy model of Raleigh damping which is characterized by C_{e} being proportional to the mass and stiffness matrices, i.e., $C_{\mathrm{e}} = \alpha M_{\mathrm{e}} + \beta K_{\mathrm{e}}$. At first, a low frequency $f = 50\,\mathrm{Hz}$ is considered. Performing 200 time steps of size $\Delta t = 5{\cdot}10^{-4}$, the vertical displacement at p_0 is recorded and depicted in the left picture of Figure 5.9. The dashed line corresponds

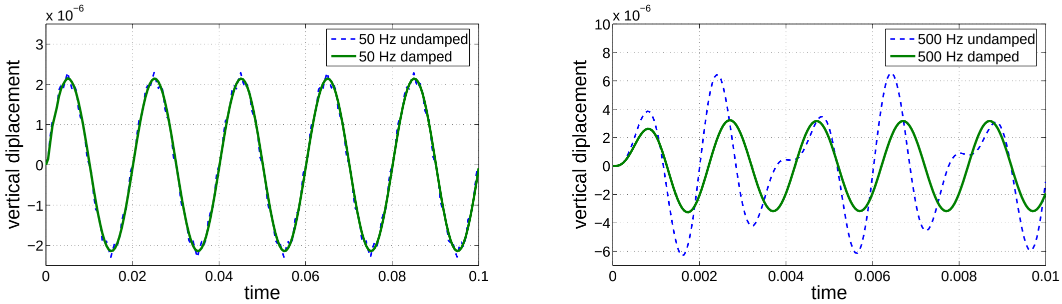

FIGURE 5.9. *Vertical displacement at* p_0 *for different frequencies of excitation:* 50 *Hz (left),* 500 *Hz (right).*

to the undamped formulation, i.e., $\alpha = \beta = 0$. The applied frequency is well below the first eigenfrequency which has been determined by the last test to be at roughly $f_0 = 720\,\mathrm{Hz}$, as depicted in the left picture of Figure 5.8. In this case, the effects of the eigenmodes can easily be damped out, resulting in the solid line exhibiting a stable sinusoidal motion. Here, the damping parameters are set to $\alpha = 2.51{\cdot}10^{1}$, $\beta = 1.59{\cdot}10^{-4}$ in Ω^{p}, and to $\alpha = 1.63{\cdot}10^{1}$, $\beta = 1.03{\cdot}10^{-4}$ in Ω^{q}, which corresponds to a loss factor of about 0.4. In a second test, the influence of the eigenmodes increases considerably for the now applied frequency $f = 500\,\mathrm{Hz}$, which is in the same range as f_0. As visualized in the right picture of Figure 5.9, the undamped motion is clearly disturbed by the lowest eigenmode. Nevertheless, it is still feasible to extract a stable sinusoidal motion at the applied frequency by employing the Raleigh damping. The parameters α, β have been adjusted in order to keep the loss factor constant, [14].

The situation becomes more critical if f is chosen to be greater than f_0. A better strategy is needed to damp out eigenfrequencies which are lower than the applied frequency. The development of such a strategy is beyond the scope of this paper.

It remains to investigate the elasto-acoustic coupling. Since the acoustic medium is chosen to be air, we can neglect the influence of the acoustic field onto the structure. Thus, the system (4.10) is decoupled by setting C_{ea} to zero in the first line of (4.10). In every time step, the structural equation is solved first, taking into account the changes in the applied electric potential. Afterwards, the acoustic response is calculated by imposing the normal velocity of the structure as inhomogeneous Neumann condition at the fluid-structure interface. For the solid, we use the same mesh as before: one layer in vertical direction of $16{\times}16$ elements in Ω^{p} and $8{\times}8$ elements in Ω^{q}, respectively, adding up to about 12000 degrees of freedom. The acoustic domain Ω^{a} is set to be a cuboid of $3\,\mathrm{m}$ width and depth, and of $1.5\,\mathrm{m}$ height, centered above the structure. On Ω^{a}, we also use quadratic Serendipity elements on a structured grid of meshsize $3/32\,\mathrm{m}$, yielding 16384 hexahedrons and about 70000 degrees of freedom. The choice of the meshsize is motivated by the expected wavelength: since the excitation frequency is set to $f = 500\,\mathrm{Hz}$, we end up with roughly 7.3 quadratic elements per wavelength, which is enough to give reasonable results. A time step size $\Delta t = 5{\cdot}10^{-5}\mathrm{s}$ is used for performing 180 time steps. Figure 5.10 shows the resulting velocity potential in four nodes p_i at distances $i{\cdot}0.1875\,\mathrm{m}$, $i = 1, \ldots, 4$, located directly above the center of the solid. As expected, the frequency coincides with the frequency of excitation by the structure. Moreover, the amplitude of the acoustic waves decreases as the distance to the vibrating structure increases. If we had to choose the meshsize conforming to the solid, namely

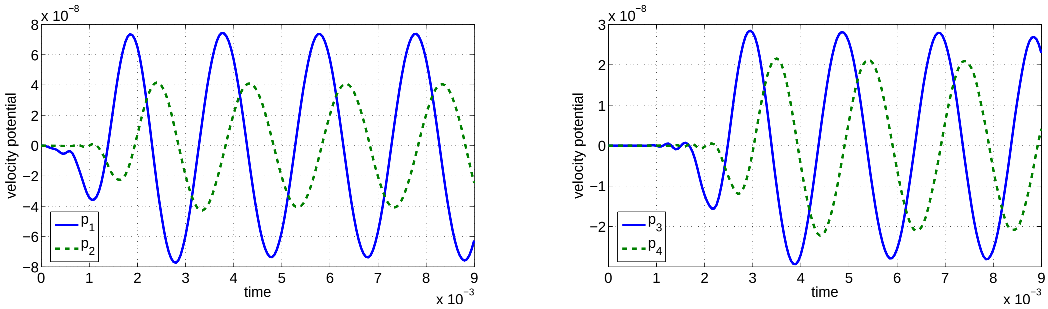

FIGURE 5.10. *Velocity potential at p_i, $i = 1, \dots, 4$, for an excitation of frequency* 500 *Hz.*

$1/200\,\mathrm{m}$, and did not want to distort the elements by coarsening them, we would end up with $(3{\cdot}200/32)^3 = (75/4)^3 > 6000$ times the number of elements for the acoustic part. This effect would become even stronger, if the wavelength increased and larger elements could be chosen to approximate the velocity potential.

6. Conclusion. In the present paper, we have investigated the coupled time dependent partial differential equations describing the interaction between the mechanical and acoustic field. We have based our formulation on the primary variables mechanical displacement and scalar acoustic velocity potential. Therewith, we can use standard Lagrangian finite elements and a symmetric coupled formulation. Our theoretical main result is the equivalence to the pure displacement based formulation on the continuous and discrete level. This equivalence allows us to employ an already available a priori analysis. On the practial side, the use of non-matching grids along the coupling interface strongly decreases the CPU time and memory consumption and furthermore improves the quality of the computational grid in each subdomain. In particular, the applicability and efficiency of our implementation has been demonstrated by three engineering examples.

REFERENCES

[1] M. Akamatsu and G. Nakamura. Well-posedness of initial-boundary value problems for piezoelectric equations. *Appl. Anal.*, 81(1):129–141, 2002.

[2] G. A. Baker and V. A. Dougalis. The effect of quadrature errors on finite element approximations for second order hyperbolic equations. *SIAM J. Numer. Anal.*, 13(4):577–598, 1976.

[3] A. Bermúdez, R. Rodríguez, and D. Santamarina. Finite element approximation of a displacement formulation for time-domain elastoacoustic vibrations. *J. Comput. Appl. Math.*, 152(1-2):17–34, 2003.

[4] C. Bernardi, Y. Maday, and A. T. Patera. Domain decomposition by the mortar element method. In *Asymptotic and numerical methods for partial differential equations with critical parameters (Beaune, 1992)*, volume 384 of *NATO Adv. Sci. Inst. Ser. C Math. Phys. Sci.*, pages 269–286. Kluwer Acad. Publ., Dordrecht, 1993.

[5] C. Bernardi, Y. Maday, and A. T. Patera. A new nonconforming approach to domain decomposition: the mortar element method. In *Nonlinear partial differential equations and their applications. Collège de France Seminar, Vol. XI (Paris, 1989–1991)*, volume 299 of *Pitman Res. Notes Math. Ser.*, pages 13–51. Longman Sci. Tech., Harlow, 1994.

[6] D. Braess. Enhanced assumed strain elements and locking in membrane problems. *Comput. Methods Appl. Mech. Engrg.*, 165(1-4):155–174, 1998.

[7] D. Braess. *Finite elements.* Cambridge University Press, Cambridge, second edition, 2001.

[8] F. Brezzi and M. Fortin. *Mixed and Hybrid Finite Element Methods.* Springer Verlag, 1991.

[9] R. Dautray and J.-L. Lions. *Mathematical analysis and numerical methods for science and technology. Vol. 5: Evolution problems I.* Springer-Verlag, Berlin, 1992.

[10] L. C. Evans. *Partial differential equations*, volume 19 of *Graduate Studies in Mathematics*. American Mathematical Society, Providence, RI, 1998.

[11] B. Flemisch, M. Kaltenbacher, and B. I. Wohlmuth. Elasto-acoustic and acoustic-acoustic coupling on non-matching grids. *Internat. J. Numer. Methods Engrg.*, 67(13):1791–1810, 2006.

[12] C. Hager and B. Wohlmuth. Analysis of a modified mass lumping method for the stabilization of frictional contact problems. Technical report, Universität Stuttgart, IANS, 2007. To appear in *SIAM J. Numer. Anal.*

[13] T. Hughes. *The Finite Element Method.* Prentice-Hall, New Jersey, 1987.

[14] M. Kaltenbacher. *Numerical Simulation of Mechatronic Sensors and Actuators*. Springer, Berlin, 2. edition, 2007.

[15] M. Kaltenbacher, R. Lerch, and G. Link. Numerical modeling of capacitive micromachined transducers. In *Computational Methods for Coupled Problems in Science and Engineering. CD-ROM Proceedings, ECCOMAS Santorini, Greece; 25.-27.05.2005.*

[16] J.-L. Lions and E. Magenes. *Non-homogeneous boundary value problems and applications. Vol. I.* Springer-Verlag, New York, 1972. Translated from the French by P. Kenneth, Die Grundlehren der mathematischen Wissenschaften, Band 181.

[17] S. Marburg and B. Nolte, editors. *Computational Acoustics of Noise Propagation in Fluids*. Springer-Verlag, Berlin Heidelberg, 2008. ISBN 978-3-540-77447-1.

[18] H. J.-P. Morand and R. Ohayon. *Fluid structure interaction*. Chichester: Wiley. Paris: Masson, 1995.

[19] N. M. Newmark. A method of computation for structural dynamics. *J. Engng. Mech. Div., Proc. ASCE*, 85(EM3):67–94, 1959.

[20] L. Olson and K. Bathe. Analysis of Fluid-Struture Interactions. A direct symmetric coupled formulation based on the fluid velocity potential. *Computer & Structures*, 21(1/2):21–32, 1985.

[21] M. Petyt. *Introduction to finite element vibration analysis*. Cambridge University Press, Cambridge, 1990.

[22] M. Rausch, R. Lerch, M. Kaltenbacher, H. Landes, G. Krump, and L. Kreitmeier. Optimization of Electrodynamic Loudspeaker-Design Parameters by Using a Numerical Calculation Scheme. *Acta Acustica*, 85(3):412–419, 1999.

[23] P.-A. Raviart and J.-M. Thomas. *Introduction à l'analyse numérique des équations aux dérivées partielles.* Collection Mathématiques Appliquées pour la Maîtrise. Masson, Paris, 1983.

[24] O. Schenk and K. G˙Solving unsymmetric sparse systems of linear equations with PARDISO. *Future Generation Computer Systems*, 20(3):475 – 487, 2004. Selected numerical algorithms.

[25] J. C. Simo and T. J. R. Hughes. On the variational foundations of assumed strain methods. *Trans. ASME J. Appl. Mech.*, 53(1):51–54, 1986.

[26] R. L. Taylor. A mixed-enhanced formulation for tetrahedral finite elements. *Internat. J. Numer. Methods Engrg.*, 47(1-3):205–227, 2000. Richard H. Gallagher Memorial Issue.

[27] A. Toselli and O. Widlund. *Domain decomposition methods—algorithms and theory*, volume 34 of *Springer Series in Computational Mathematics*. Springer-Verlag, Berlin, 2005.

[28] W. Voigt. *Lehrbuch der Kristallphysik*. Teubner, 1910.

[29] B. I. Wohlmuth. A mortar finite element method using dual spaces for the Lagrange multiplier. *SIAM J. Numer. Anal.*, 38(3):989–1012, 2000.

B. Flemisch
Universität Stuttgart, IWS
Pfaffenwaldring 61
70569 Stuttgart
Germany
E-Mail: bernd@iws.uni-stuttgart.de

M. Kaltenbacher
Alpen-Adria University of Klagenfurt
Institute of Smart Systems Technologies
Universitätsstraße 65-67
9020 Klagenfurt
Austria
E-Mail: manfred.kaltenbacher@uni-klu.ac.at

S. Triebenbacher
Alpen-Adria University of Klagenfurt
Institute of Smart Systems Technologies
Universitätsstraße 65-67
9020 Klagenfurt
Austria
E-Mail: simon.triebenbacher@uni-klu.ac.at

B. Wohlmuth
Universität Stuttgart, IANS
Pfaffenwaldring 57
70569 Stuttgart
Germany
E-Mail: barbara.wohlmuth@ians.uni-stuttgart.de

Erschienene Preprints ab Nummer 2009/001

Komplette Liste: `http://preprints.ians.uni-stuttgart.de`

2009/001 *Sändig, A.-M.:* Nichtlineare Funktionalanalysis mit Anwendungen auf partielle Differentialgleichungen, Vorlesung im Wintersemester 2008/09

2009/002 *Kissling, F., LeFloch, P. G., Rohde, C.:* A kinetic decomposition for singular limits of non-local conservation laws

2009/003 *Haink, J., Haspot, B., Rohde, C.:* Existence of global weak solutions for boundary value problems for compressible fluid models with nonlocal capillary tensor

2009/004 *Flemisch, B., Kaltenbacher, M., Triebenbacher, S., Wohlmuth, B. I.:* The equivalence of standard and mixed finite element methods in applications to elasto-acoustic interaction